Unclassified

SECURITY CLASSIFICATION OF THIS PAGE (When Data Entered)

| REPORT DOCUMENTATION PAGE | READ INSTRUCTIONS BEFORE COMPLETING FORM |
|---|---|
| 1. REPORT NUMBER: RADC-TR-79-247 (14) | 2. GOVT ACCESSION NO.: AD-A085570 | 3. RECIPIENT'S CATALOG NUMBER |
| 4. TITLE (and Subtitle): DETECTION OF RADAR SIGNAL MODULATIONS INDUCED BY TARGET AIRCRAFT STRUCTURAL VIBRATIONS (6) | 5. TYPE OF REPORT & PERIOD COVERED: In-House Report |
| | 6. PERFORMING ORG. REPORT NUMBER |
| 7. AUTHOR(s): John F. Lennon (10) | 8. CONTRACT OR GRANT NUMBER(s) |
| 9. PERFORMING ORGANIZATION NAME AND ADDRESS: Deputy for Electronic Technology (EEC) Hanscom AFB Massachusetts 01731 | 10. PROGRAM ELEMENT, PROJECT, TASK AREA & WORK UNIT NUMBERS: (16) 23050404 (17) J4 |
| 11. CONTROLLING OFFICE NAME AND ADDRESS: Deputy for Electronic Technology (EEC) Hanscom AFB Massachusetts 01731 (11) | 12. REPORT DATE: Sep[redacted]79 |
| | 13. NUMBER OF PAGES: 59 |
| 14. MONITORING AGENCY NAME & ADDRESS(if different from Controlling Office): (9) Technical repts | 15. SECURITY CLASS. (of this report): Unclassified |
| | 15a. DECLASSIFICATION/DOWNGRADING SCHEDULE |

16. DISTRIBUTION STATEMENT (of this Report)

Approved for public release; distribution unlimited.

17. DISTRIBUTION STATEMENT (of the abstract entered in Block 20, if different from Report)

(12) 60

DTIC ELECTE JUN 16 1980 D

18. SUPPLEMENTARY NOTES

19. KEY WORDS (Continue on reverse side if necessary and identify by block number)

Radar signature
Radar cross section, dynamic
Power spectra
Signal modulation
Electromagnetics

20. ABSTRACT (Continue on reverse side if necessary and identify by block number)

The possibility of aircraft identification using radar signal modulations induced by target airframe vibrations is analyzed. Emphasis is placed on detectability of the signal modulation, but attention is given to dependence on the angle of incidence since a major concern is identification at angles where engine effects are not observable. The approach is to compare the strength of the backscatter modulation relative to the unmodulated signal from the aircraft.

Since it is the modulation of the signal that is significant, and not the exact radar cross section, a simple wire model representation of the aircraft is used. → over

DD FORM 1 JAN 73 1473 EDITION OF 1 NOV 65 IS OBSOLETE

Unclassified

SECURITY CLASSIFICATION OF THIS PAGE (When Data Entered)

30915'0 xlk

20. (Cont)

The radar backscatter results at 7 MHz and 28 MHz are calculated using a modified method-of-moments solution. The method employs successive static electromagnetic scattering solutions from a target where the position of the wing has been changed between calculations. The results are considered as discrete samples of the continuous, modulated signal. The power of the modulation is then estimated by determining the relative power spectra of the modulated signal. An approach that explicitly derives continuous time dependent scatter is included. This uses a simple crossed dipole theory with wing dipole oscillations. The Dipole model, however, requires external information on the location of the appropriate scattering centers along the dipoles. Since this is incident angle dependent, the model becomes cumbersome.

For all cases, the power in the modulation is extremely weak. Translated into range, the results indicate that the aircraft would have to approach to within one-tenth its maximum detection distance before the modulation would be visible. The angular variation in the results would indicate that their use in identification would be complicated. Although this study is a limited one, its conclusions of angular variability and stringent range limitations strongly suggest that further investigation of structural vibrations would not be reasonable, as far as application to tactical aircraft identification is concerned.

## Preface

The author gratefully acknowledges the contributions of Dr. John K. Schindler whose comments, suggestions, and constructive criticism were invaluable and of Dr. Richard R. Mack who originally suggested this problem when a member of this organization.

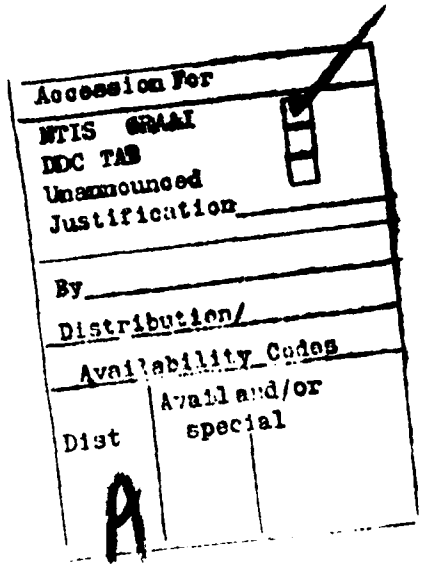

## Contents


| | | |
|---|---|---|
| 1. | INTRODUCTION | 9 |
| | 1.1 Background | 9 |
| | 1.2 Approach | 10 |
| | 1.3 Scope | 11 |
| 2. | PROCEDURES | 12 |
| | 2.1 Radar and Target Parameters | 12 |
| | 2.2 Scattering Model | 12 |
| | 2.3 Power Spectra | 23 |
| 3. | RESULTS | 26 |
| | 3.1 Backscatter Patterns | 26 |
| | 3.2 Scatter Modulation and Power Spectra | 27 |
| 4. | DIPOLE MODEL | 48 |
| | 4.1 Theoretical Analysis | 48 |
| | 4.2 Comparison of Results | 50 |
| | 4.3 Discussion | 53 |
| 5. | CONCLUSIONS | 54 |
| | 5.1 Related Results | 54 |
| | 5.2 Present Results | 55 |
| | 5.3 Assessments | 56 |
| REFERENCES | | 57 |
| LIST OF SYMBOLS | | 59 |

## Illustrations


1. Model of F-111 Type Aircraft Using Crossed Wires 13
2. Scattering Coordinate System for the Method-of-Moments Solution 14
3. The Dependence of 7-MHz Backscatter Magnitude Patterns on Wire Radius 15
4. Seven-MHz Backscatter Phase Patterns 18
5. The Dependence of 28-MHz Backscatter Magnitude Patterns on Wire Radius 19
6. Twenty-eight-MHz Backscatter Phase Patterns 22
7. Azimuthal Variation of 7-MHz,$E_\phi$ Polarized Backscatter Modulation 28
8. Azimuthal Plane Power Spectra of 7-MHz,$E_\phi$ Polarized Modulated Backscatter 29
9. Azimuthal Variation of 7-MHz,$E_\theta$ Polarized Backscatter Modulation 31
10. Azimuthal Plane Power Spectra of 7-MHz,$E_\theta$ Polarized Modulated Backscatter 32
11. Azimuthal Variation of 28-MHz,$E_\phi$ Polarized Backscatter Modulation 33
12. Azimuthal Plane Power Spectra of 28-MHz,$E_\phi$ Polarized Modulated Backscatter 34
13. Azimuthal Variation of 28-MHz,$E_\theta$ Polarized Backscatter Modulation 35
14. Azimuthal Plane Power Spectra of 28-MHz,$E_\theta$ Polarized Modulated Backscatter 37
15. Effect of Elevation Angle on 7-MHz,$E_\theta$ Polarized Backscatter Modulation 38
16. Elevation Plane Power Spectra of 7-MHz,$E_\theta$ Polarized Modulated Backscatter 40
17. Effect of Elevation Angle on the Signal Modulation and Power Spectra of 7-MHz,$E_\phi$ Polarized Backscatter 41
18. Effect of Elevation Angle on 28-MHz,$E_\theta$ Polarized Backscatter Modulation 42
19. Elevation Plane Power Spectra of 28-MHz,$E_\theta$ Polarized Modulated Backscatter 43
20. Effect of Elevation Angle on the Signal Modulation and Power Spectra of 28-MHz,$E_\phi$ Polarized Backscatter 44
21. Azimuthal Plane Variation of the Signal Modulation and Power Spectra of 7-MHz,Cross-polarized Backscatter 46
22. Azimuthal Plane Variation of the Signal Modulation and Power Spectra of 28-MHz,Cross-polarized Backscatter 47
23. Model Configuration for the Dipole Theory 48
24. Comparison of Method-of-Moments and Dipole Model Backscatter Magnitude Patterns at 7 MHz 51
25. Comparison of the Modulated Backscatter Results for Both Models 52
26. The Effect of Azimuth on the Currents Induced on the Model Wires in the Method-of-Moments Calculation 53

# Tables

1. Detection Range as a Function of Relative Power 25

# Detection of Radar Signal Modulations Induced by Target Aircraft Structural Vibrations

## 1. INTRODUCTION

### 1.1 Background

This report addresses some aspects of the following question: Are there aircraft motions (other than engine component rotations)[1] which induce modulations on the target radar return that would be suitable for use as an identifier? One reason for considering this subject is that engine identification is aspect-angle limited; modulations based on other sources may be visible at additional azimuthal angles. An analysis has been made of one possible modulation source, namely, airframe vibrations induced by atmospheric gusts or turbulence. This particular aspect was suggested initially by earlier radar detection of agitated metals (RADAM)[2] studies which, in part, dealt with structural motions and vibrations induced by external forces.

The concept of identification includes aspects of detection, uniqueness, and recognition. A program directed to the study of aeroelastic airframe motions for identification must consider these factors. The first aspect, detection, has been

(Received for publication 11 September 1979)

1. Hynes, R., and Gardner, R.E. (1967) Doppler spectra of S-band and X-band signals, Supplement to IEEE Trans. Aerospace and Electrical Systems AES-3:356-365.
2. Newburgh, R.G. (1978) Basic Investigations of the Radam Effect, RADC-TR-78-151, AD A058099.

examined by the RADC Electromagnetic Sciences Division. The question is whether these motions will induce corresponding radar signal modulations over a range of azimuth angles that are sufficiently strong to be detectable. The second aspect, uniqueness of signature, was investigated by the University of Michigan,[3] with concentration on characterizing the induced motions and examining the variations with aircraft type and operational configuration. For typical tactical aircraft, vibrational frequencies, mode shapes, and airframe displacements have been established for different aircraft velocities, wing aspect, fuel loads, and external stores. The results show considerable variability. The third aspect, recognition, is concerned with resolving signature elements from the radar observables. Since this aspect depends on results from the first two areas, its discussion has been deferred.

### 1.2 Approach

The major emphasis of the present work is on estimating the strength and angular variation of radar signal modulations induced by airframe motions. It is not concerned with generating specific characteristic patterns. This limited goal represented a major factor in deciding how the problem would be approached. For example, the scattering pattern does not have to correspond exactly to that of a given target; an approximate representation of the differences between the modulated radar signal and the return from the target with no structural motion is sufficient. We decided to modify an existing computer program developed under contract by Syracuse University.[4] This program treats the radiation and scattering from configurations of arbitrarily bent thin wires. The modification would restructure the scattering version of the program to include the modulation. To represent modulation, the solution must describe scattering from a target whose properties are varying with time. In this study, time dependence is simulated by obtaining successive static scattering solutions, changing the target configuration for each calculation. The sequence of static results is considered to represent discrete samples of a continuous signal from a target with superimposed structural oscillations.

Lin and Richmond[5] describe a series of measurements and calculations for four aircraft wire models of increasing complexity. For target length to wavelength

---

3. Anderson, W.G., Sengupta, D., and Correa, S. (1979) Inflight Aircraft Vibration Modes and their Effect on Aircraft Radar Cross-Section, RADC-TR-79-72.

4. Kuo, D.C., and Strait, B.J. (1972) Improved Programs for Analysis of Radiation and Scattering by Configurations of Arbitrarily Bent Thin Wires, AFCRL-TR-75-0051, AD 739203.

5. Lin, Y.T., and Richmond, J.H. (1975) EM modeling of aircraft at low frequencies, IEEE Trans. Antennas and Propagation AP-23:53-56.

ratio, $L/\lambda \sim 0.8$ and 1.4, they show scattering results in the yaw plane for a signal polarized in the $\phi$ direction, $E_\phi$. For the simple model, they do not feel the agreement is sufficient; the calculation and measurements diverge at the higher frequency at an azimuthal angle $\phi \sim 110°$ where measurements show a deep null; also, agreement at larger angles is sporadic. The lower frequency results, however, and the results near nose-on at the higher frequency do show some consistency in the form of the scattering pattern. Further, the patterns for the simple model and for a very complex one do not differ significantly. These factors bear on the use of the simple wire model of the present study where we are concerned only with showing relative trends. The frequencies we use are 7 MHz and 28 MHz; these correspond to $L/\lambda$ of 0.5 and 2.0, respectively. At S-band or higher frequencies, the simple wire model for the aircraft would not be a reasonable one, but a general assessment of the relative strength of the effect is possible from results at the present frequencies.

It should be noted that the University of Michigan report includes a limited electromagnetic study at higher frequencies ($\lambda$ = 30 cm and $\lambda$ = 3 m) as an adjunct to the vibrational analyses. The characteristic structural motions of one aircraft were translated into relative scattering center motion and some time-varying cross-section results were obtained. This is discussed in Section 5.1.

### 1.3 Scope

The goals and limitations that defined the bounds of the program have been discussed. Within this framework, the steps of the procedure can be outlined. The first step consists in looking at the complete unmodulated backscatter patterns at the two frequencies. Next, the variation in the scattered signal as a result of simulating the target vibration is obtained from a succession of static backscatter calculations for a wide range of viewing angles. (There is no inherent limitation to the motions which can be included, but for simplicity, only wing vibration is studied.) The scattering results show the variations in phase and magnitude that occur for one cycle of the periodic wing deflections of the target. Then, in order to estimate the relative power of this modulated return as compared to an unmodulated signal, the output is transformed into the frequency domain. The power contained in the non-zero frequency components represents the potential detectability of the induced modulation.

The preceding objectives are the main themes of the study but one additional aspect is included (Section 4). An attempt is made to show a relation between the results obtained using sequential static solutions and results based on a more simplistic model which does, however, include variations in wing position in its formulation. Each of these subjects will be discussed.

## 2. PROCEDURES

### 2.1 Radar and Target Parameters

The first parameters which have to be determined are those needed to specify the electromagnetic scattering from the target. These include aircraft considerations and radar aspects.

The F-111 fighter bomber used in the study has a 19-m wingspan and a 22-m over-all length. For purposes of modeling with a configuration of wires, the wing wires are taken as joining the fuselage wires at the midpoint of the aircraft. For the calculations in this report, the wing tip deflection was taken to be 5 cm peak to peak.

The frequencies selected are in the HF band. For that frequency range, we can consider the case of over-the-horizon radar surveillance. Polarization is random. Angles of incidence on the aircraft are between 60° and 85° from vertical. The signal has a waveform repetition rate of 50 Hz. Coherent integration times of 1 sec are typical. At a 6-Hz wing oscillation rate assumed for the aircraft, these values are consistent with 8 pulses or samples of the scattered-field complex amplitudes per vibration cycle.

### 2.2 Scattering Model

The next topic to be discussed is the scattering model. As pointed out in the introduction, the computer program and theory were originally developed by Syracuse University and a modified version of their program was applied to the present problem. Various aspects of the program and theory have been described in detail in a number of reports[4,6] and articles.[7,8] A summary of the theory, the application of the program to this problem, and the program modifications will be discussed.

The formulation is an application of the method of moments to configurations of thin wires irradiated by a plane electromagnetic wave. The wires are assumed to be perfect conductors. A piecewise linear current approximation is assumed along each wire which is divided into subsections for the analysis. The currents are restricted to flow axially. At the ends of the wires, the currents are zero. At

---

6. Chao, H. H., and Strait, B. J. (1970) Computer Programs for Radiation and Scattering by Arbitrary Configurations of Bent Wires, AFCRL-TR-70-0374, AD 713156.

7. Harrington, R. D. (1967) Matrix methods for field problems, Proc. IEEE 55:136-149.

8. Chao, H. H., Strait, B. J., and Taylor, C. D. (1971) Radiation and scattering by configuration of bent wires with junctions, IEEE Trans. Antennas and Propagation AP-19:701-702.

junctions, continuity of potential and Kirchhoff's current law are satisfied; note that the current does not have to be continuous across the junction. In a Galerkin solution, triangle functions are used for both the current and test expansion functions. The integro-differential equations reduce to equations which require matrix inversion to solve for wire current distributions. The generalized voltage matrix, or source term, is obtained using characteristics of the incident wave. The current distribution matrix for the wire configuration permits calculation of the scattered field from the target.

The thin wire assumption places some limitations on the wire model dimensions. For each of the four wires, the cross sectional radius "a" has to satisfy the relations $L/a >> 1$ and $a << \lambda$. At least twenty segments, $\ell_s$, are required per wavelength. The resulting configuration for f = 7 MHz can be seen in Figure 1. (Additional segments are required at f = 28 MHz.) The program requires an even number of segments on each wire. The overlapping segments at the junction represent a mathematical requirement for the current equations; it is not a case of separate wires with capacitive coupling.

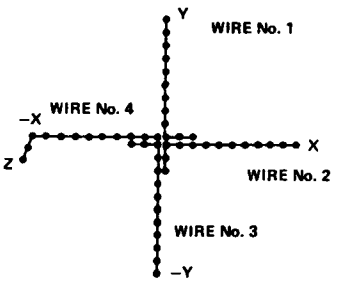


Figure 1. Crossed Wire Configuration Showing 7-MHz Point Spacing

Figure 2 shows the orientation of the model and incident field vector $\hat{k}$. The azimuth angle $\phi$ and elevation angle $\theta$ are indicated, as are the polarization vectors $\hat{e}_\phi$ and $\hat{e}_\theta$. The rear fuselage wire has a short vertical tail and the variable wing-wire zy-plane coordinate positions needed to include vibration are shown as the shaded segments. The incident fields $E_\phi$ and $E_\theta$ are each considered to be unit vectors with magnitudes of 1 V/m. The phase of the incident wave is referenced to the origin of the coordinate system.

The thin wire assumption as applied to the present case does not allow exact scaling of the cross-sectional areas of the aircraft components. The need is to obtain results that are essentially independent of wire radius changes. The values of the wing and vertical tail segments are one-twelfth the radius of the corresponding fuselage elements.

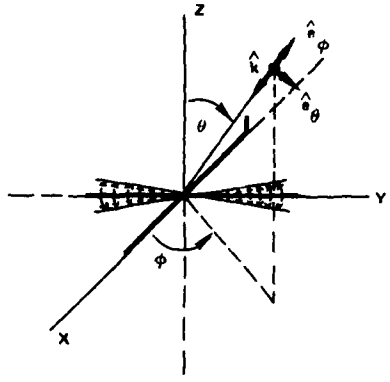


Figure 2. Scattering Model Coordinate System for the Method-of-Moments Solution Showing Scattering Angles and Polarization Vectors

Using results that do not change with radius eliminates any pecularities in the solution associated with a particular relation of frequency, length, and model radius which would not be appropriate in general. Thus, to confirm that solutions were not dependent on the cross sectional radius, limits from the thin wire and segment length-to-radius constraints were tested by successively decreasing the radius until convergence was established. The various backscatter patterns for the two frequencies as a function of cross-sectional radius are shown in Figures 3 to 6.

Figure 3 shows the copolarized backscatter magnitudes for $E_\phi$ and $E_\theta$ polarized incident waves at 7 MHz. Magnitude is plotted as a function of elevation angle for successive azimuthal angles. The results of decreasing radius is clear. Convergence is satisfactory for fuselage wire radius, $a \leq 0.0019$ m. Figure 4 shows the corresponding phase patterns for the convergent radius solutions.

Figure 5 shows the copolarized backscatter magnitudes at 28 MHz. The change in wavelength alters the pattern structure. Convergence at that frequency is obtained at $a \leq 0.00096$ m. Figure 6 shows the corresponding phase patterns at 28 MHz.

Modifications to the original Syracuse program fall into three main categories: The first represents generalization of the program beyond its original format; the second is the cycling of the entire program to obtain the sequential solutions needed for the modulation aspect; the third alteration is the addition of the new subprogram which takes the output of the modulated backscatter calculations and generates the appropriate power spectra. This last aspect is an addendum rather than an internal change and its discussion will be deferred to Section 2.3, since it is a part of that major phase of the over-all effort.

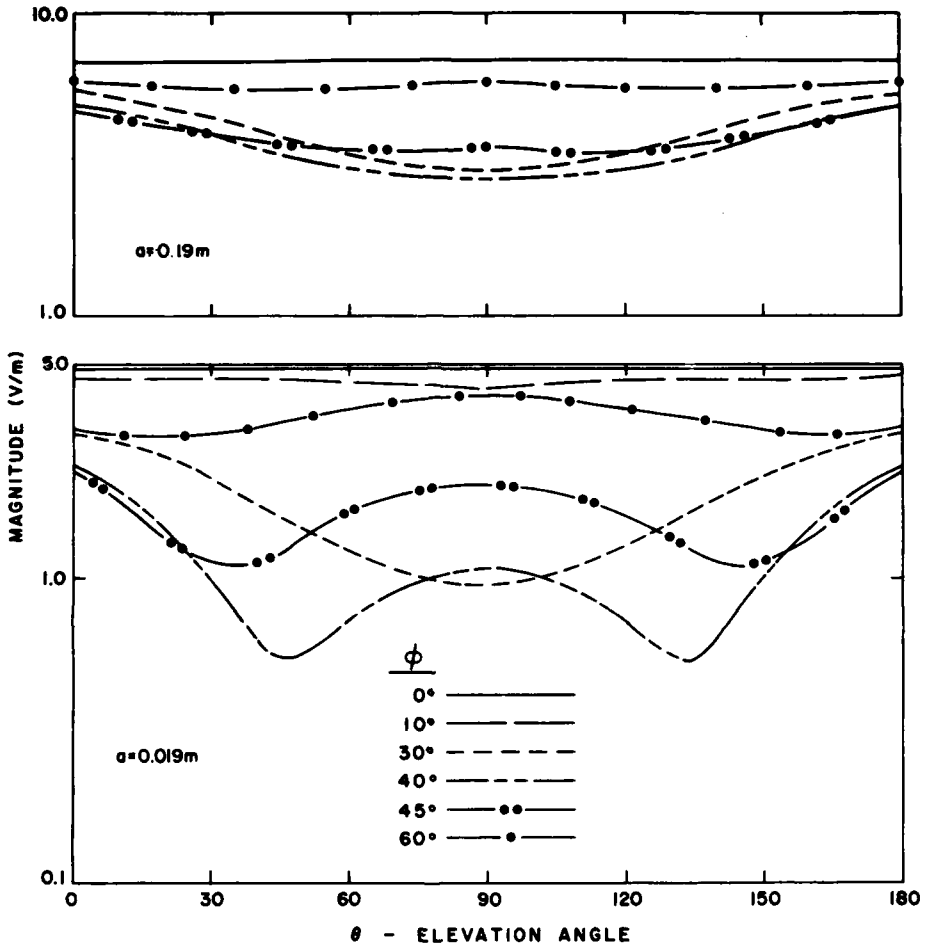


(a)

Figure 3. Seven-MHz Elevation Plane Backscatter Field Magnitudes for Successive Values of Wire Radius: (a) $E_\phi$ polarization, a = 0.19 m, and a = 0.019 m; (b) $E_\phi$ polarization, a = 0.0019 m; (c) $E_\theta$ polarization, a = 0.0019 m

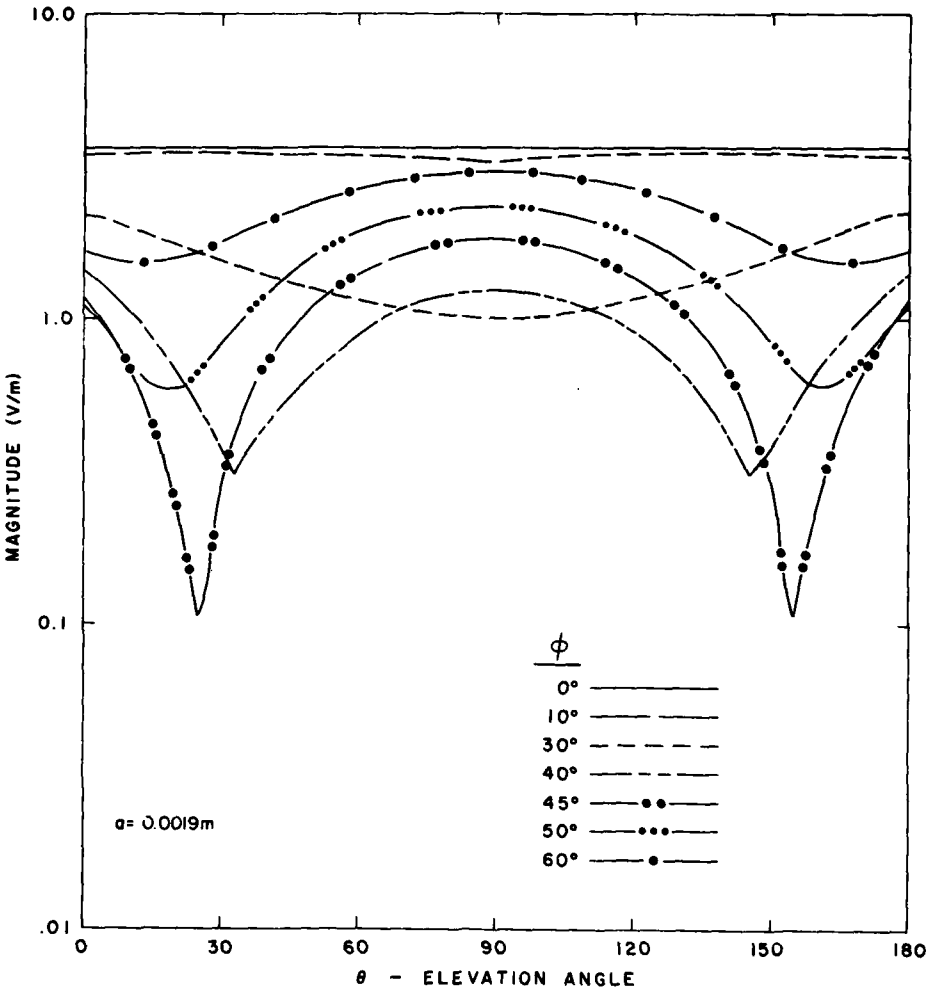


(b)

Figure 3. (Cont)

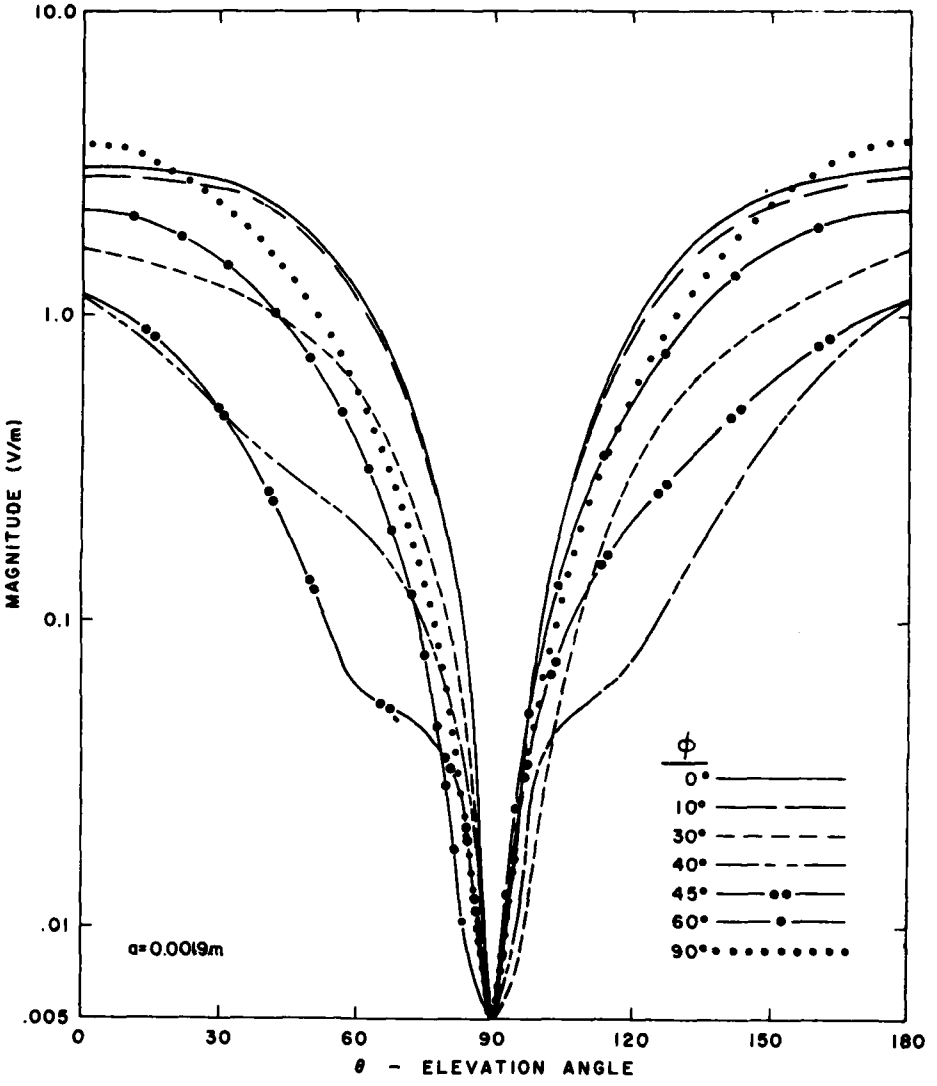


(c)

Figure 3. (Cont)

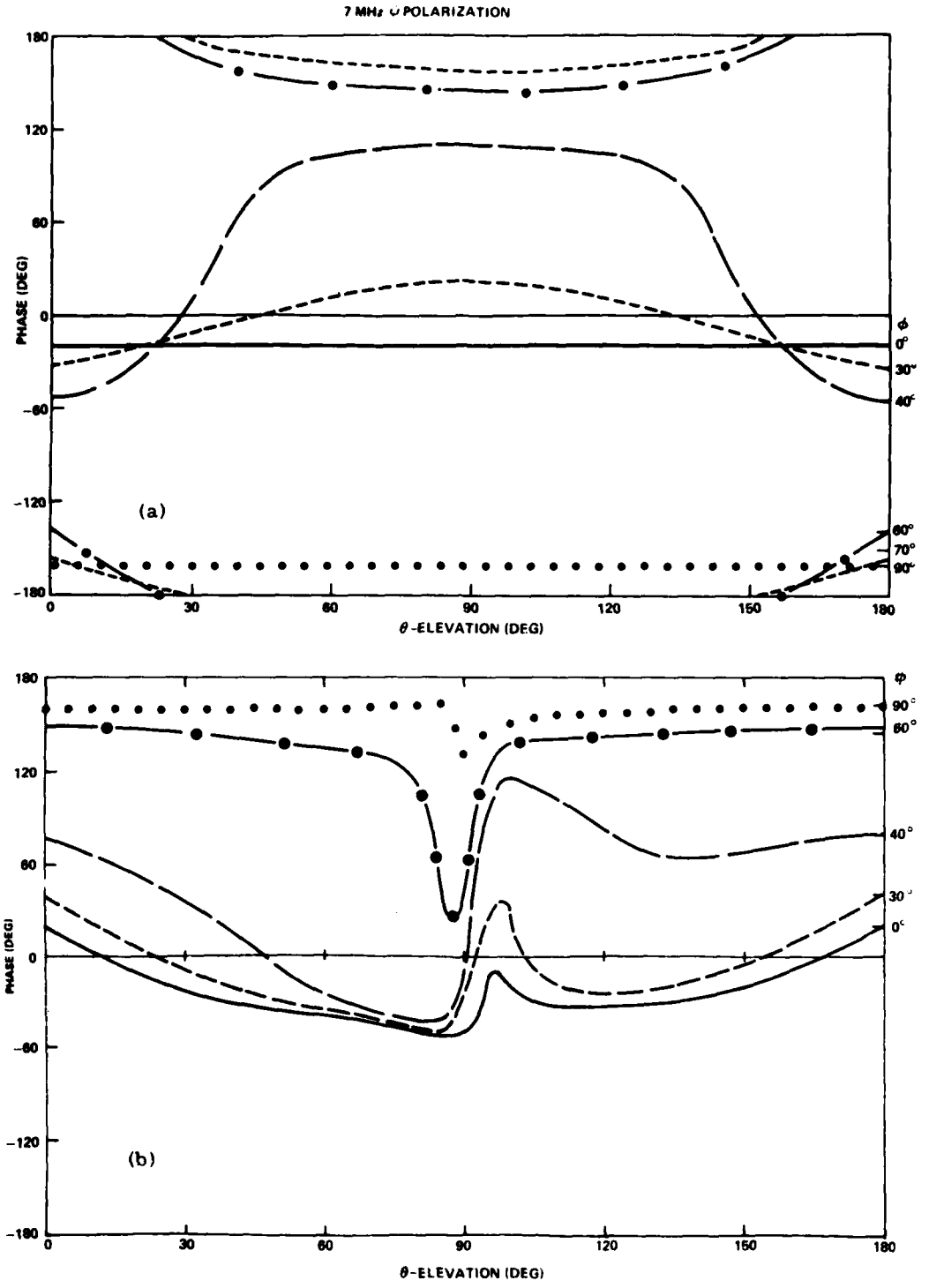


Figure 4. Seven-MHz Elevation Plane Backscatter Field Phase Values for a = 0.0019 m: (a) $E_\phi$ polarization and (b) $E_\theta$ polarization

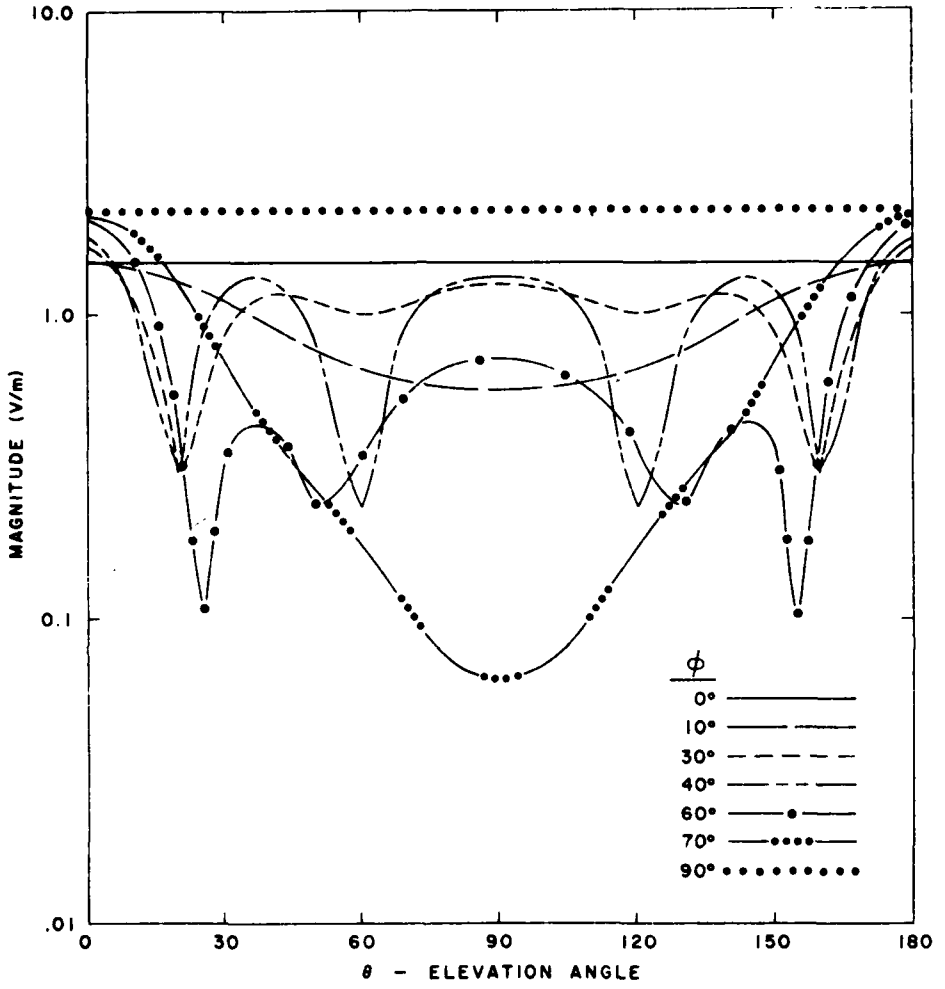


(a)

Figure 5. Twenty-eight-MHz Elevation Plane Backscatter Field Magnitudes for Successive Values of Wire Radius: (a) $E_\phi$ polarization, a = 0.019 m; (b) $E_\phi$ Polarization, a = 0.0019 m (curves) and a = 0.00096 m (symbols); (c) $E_\theta$ polarization, a = 0.0019 m (curves) and a = 0.00096 m (symbols)

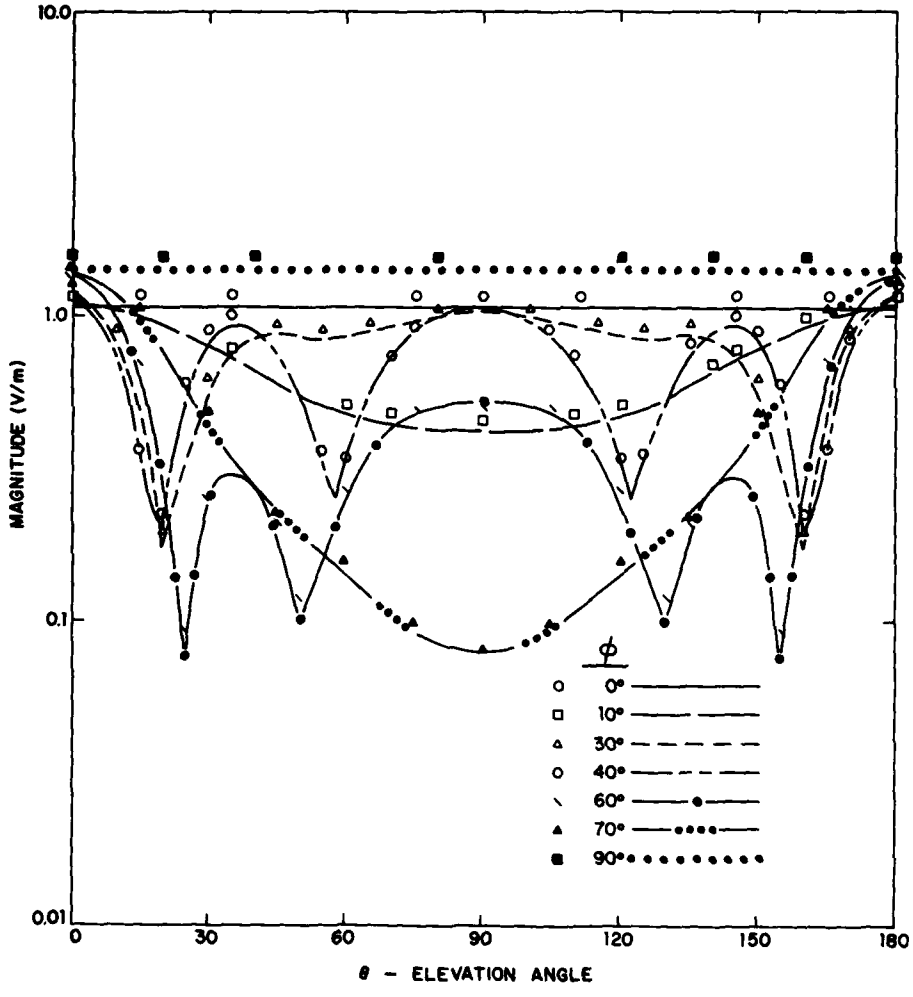


(b)

Figure 5. (Cont)

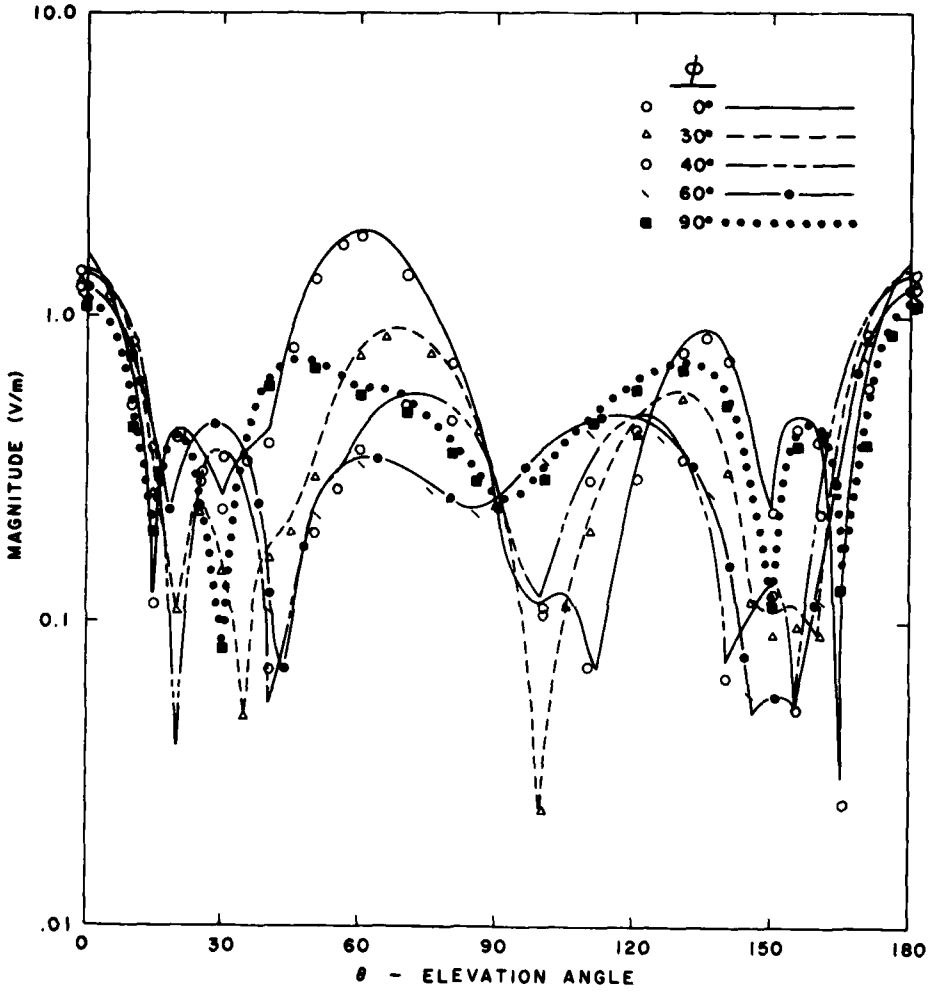


(c)

Figure 5. (Cont)

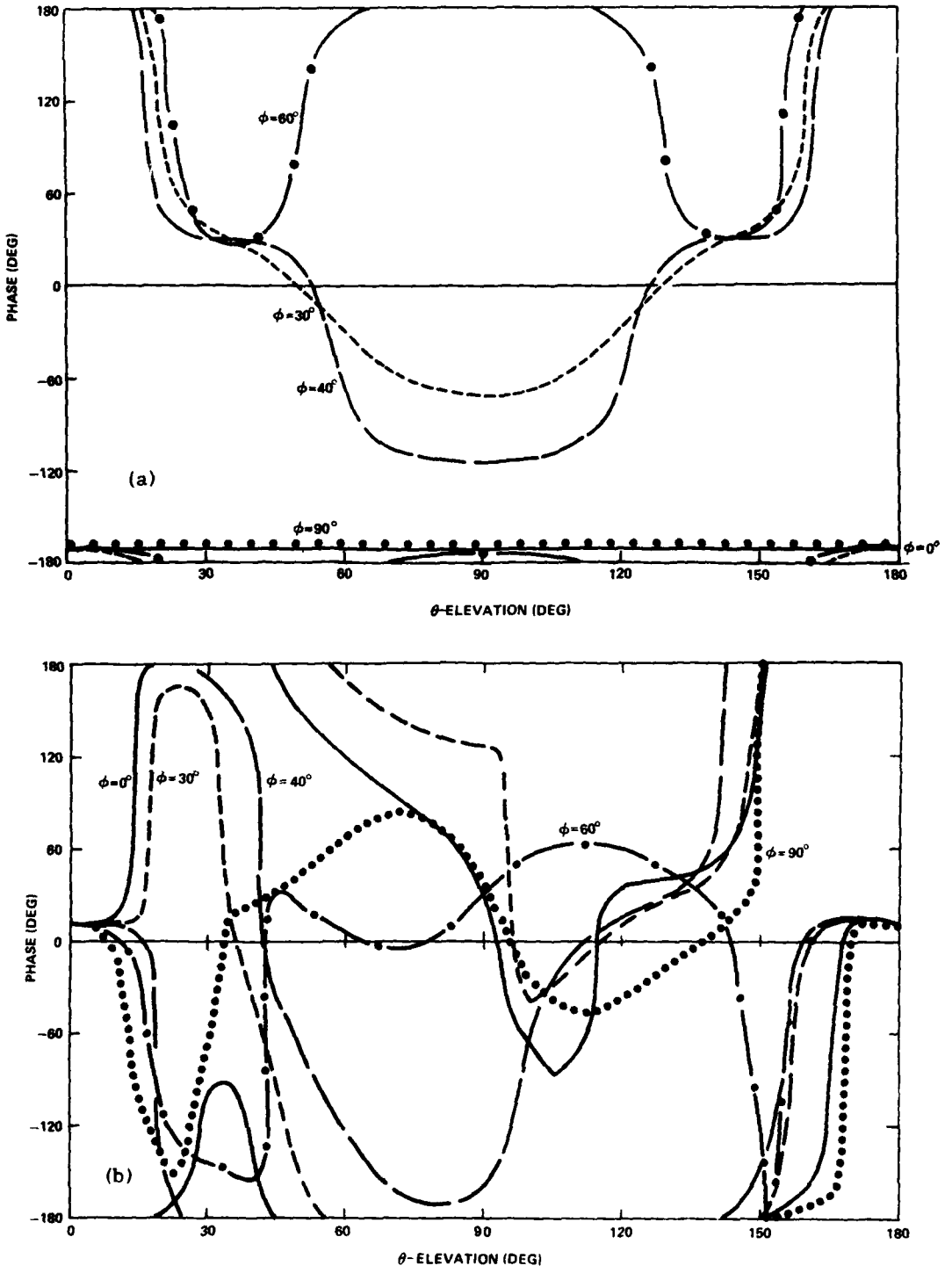


Figure 6. Twenty-eight-MHz Elevation Plane Backscatter Field Phase Values for a = 0.00096 m: (a) $E_\phi$ polarization; (b) $E_\theta$ polarization

The changes which make the program more general are not major ones and they do not significantly affect the present problem. The dimensions of the computer program variables have been increased to handle the increased number of points on the wires required for signal frequencies and segment lengths. There is a new capability to verify that the correspondingly larger matrices are being inverted properly. Also, more flexibility has been given to the possible sequencing of input cases and output angles for which fields are calculated.

The inclusion of a changing target, on the other hand, does involve a basic change in the program's orientation. In the original version, a specific target is irradiated by a given sequence of incident waves and the corresponding scattered fields are determined. To examine signal modulation, a signal incident wave is scattered by successively altered wire configurations representing the changing wing coordinates. The backscatter history of the vibrating target can be seen in the outputs. This basic change to the program was relatively simple to incorporate because of the modular structure of the original program format. The calculations are done in various subroutines and the main program serves to control data input and output. Thus, changes like the present one which need repeated calculations essentially affect only the main program; the various calculational routines are unchanged. The final addition to the program involves collecting the results of the sampled scattered-field calculation as a function of wing deflection for each azimuth and elevation. The regrouped results serve as input to the power spectrum calculation which will be discussed in the next section.

### 2.3 Power Spectra

The previous section has outlined the steps that determine the variation with time of the magnitude and phase of the backscatter due to wing deflection. The next question is: How to measure this modulation in terms of its relative power? Since the strength of a signal determines the distance at which it can be detected, this can also be translated into terms of a modulation detection range, an appropriate measure for radar problems. Both aspects will be discussed. The sequence of material is a general discussion of the method, the relation to the radar-range equation, and finally the approach used in the computer program to obtain the estimates.

One approach to analyzing a signal that is represented as a function of time f(t) is to Fourier transform it and examine the frequency domain content of the signal $F(\omega)$. The corresponding power spectra of the signal $P(\omega) \alpha |F(\omega)|^2$. For application to the present case, consider that the Fourier transform of a constant time function is a delta function in the frequency domain. The power then, is based on the square of the amplitude associated with the delta function. If the signal varies

with time as a result of an impressed modulation, then the frequency domain pattern, no longer a delta function, will contain additional terms representing the contribution of the modulation. In this present formulation, discrete time samples of the signal are used; this corresponds to the intrinsic sampling for a pulsed radar. The appropriate transform for sampled data is the discrete Fourier transform:

$$F_i = (1/N)\sum_{s=0}^{N-1} f_s \, e^{-j[2\pi i (sT)/(NT)]}$$

for

$$i = 0, 1, \ldots, N-1 ,$$

where

$$f_s = f(sT)$$

and

T = sample period.

The corresponding member of the transform pair is

$$f_s = \sum_{i=0}^{N-1} F_i \, e^{j[2\pi i (sT)/(NT)]}$$

for

$$s = 0, 1, \ldots, N-1 .$$

The relative power of the signal modulation can be expressed in terms of radar analysis. The radar range equation can be used to determine the detection range for each modulation component. This allows us to assess each component's usefulness for target classification. We require the signal-to-noise ratio to be constant for constant detectability. This implies that the ratio of cross section to range raised to the fourth power, $\sigma / R^4$, is also constant for the two signals. The power of a signal in terms of the maximum range at which it can be detected is $[\sigma_0 / R^4_{max}]$. Then the equivalent detectability of the modulation requires

$$[\sigma_{mod}/R^4_{mod}] = [\sigma_0/R^4_{max}]$$

or

$$R^4_{mod} = (\sigma_{mod}/\sigma_0)\, R^4_{max} .$$

We now introduce the relative power of the modulation components $\sigma_{mod}/\sigma_0$ expressed in terms of dB. This leads to a convenient form for the range at which a given modulation component can be detected compared to the range at which the unmodulated target is detectable.

$$R_{mod}/R_{max} = 10^{[\sigma_{mod}/40\,\sigma_0]}$$

Table 1 shows a correspondence between relative power in dB and detection range.

Table 1. Detection Range as a Function of Relative Power

| Relative Power (dB) $\sigma_{mod}/\sigma_0$ | $R/R_{max}$ |
|---|---|
| -30 | 0.18 |
| -40 | 0.10 |
| -50 | 0.03 |

The power spectra determination has been added to the scattering program. For each incident wave the sequential backscatter field results for the selected propagation directions are used as input to a fast Fourier transform program suggested by Uhrich.[9] For convenience, a single cycle of wing oscillation is examined. Both copolarized and cross-polarized scattering are considered. The output power spectra terms are normalized with respect to the transform of the unmodulated signal. This shows the strength of the modulation.

The various analytical techniques used in the study have been described. The next topic relates to results.

9. Uhrich, M. L. (1969) Fast Fourier transforms without sorting, IEEE Trans. Audio and Electroacoustics AU-17:170-172.

## 3. RESULTS

The results can be divided into two areas: The first is the unmodulated overall backscatter patterns for the two frequencies; the second is the phase, amplitude, and power spectra for selected cases with signal modulation.

### 3.1 Backscatter Patterns

The aim of this research is to study the detectability and variability of signal modulation as a function of angle of incidence of the radar signal. The first step in understanding these factors is to consider the nature of the complete unmodulated backscatter patterns at the two frequencies. These results serve to place the more detailed modulation studies in perspective. Figures 3 through 6 show the magnitude and phase of the backscatter signal when the wing is fixed in the horizontal plane. At each of the two frequencies, the two signal polarizations are presented.

For 7 MHz, the $E_\phi$ polarized magnitude pattern has a peak in the elevation plane at $\theta = 90°$ and nulls at $\theta = 30°$ and 150°. This can be seen from Figure 3b. In the azimuthal plane, there is a minimum at $\phi = 30°$. (This repeats at $\phi = 120°$.) The elevation plane nulls are deeper. The phase plots of Figure 4b show sensitivity at $\theta = 30°$ and 150° in the elevation plane patterns.

The $E_\theta$ polarized magnitude pattern depicted in Figure 3c shows a strong null for all the azimuthal cases in the vicinity of $\theta = 90°$. There is a minimum in the azimuthal plane pattern near $\phi = 45°$, but the elevation plane result is far stronger. In Figure 4b, the phase variations show a corresponding sensitivity near the yaw plane, $\theta = 90°$; there is a phase change reflecting the azimuthal null as well.

For the shorter wavelength case, 28 MHz, the patterns are more complex, as would be expected. The $E_\phi$ backscatter magnitude results, shown in Figure 5b, have nulls in the elevation plane patterns near $\theta = 30°$, 60°, 120°, and 150°. The azimuthal plane minima appear in the vicinity of $\phi = 20°$ and 70°. They are lower relative to the peaks than was the case at 7 MHz. The phase pattern variations conform to the nulls from both planes for this case, as can be seen in Figure 6a.

The $E_\theta$ polarized magnitudes are the most complex patterns, as seen in Figure 5b. The elevation plane results have numerous nulls and the spacing is not identical for all azimuth positions. The main nulls appear in the vicinity of $\theta = 20°$, 110°, and 150°. The azimuthal plane patterns have a minimum near $\phi = 60°$. The elevation plane nulls are deeper than those in the azimuthal plane. The phase variations, shown in Figure 5b, are as complex as the magnitudes. Strong changes in phase appear to be occurring in conjunction with the elevation plane magnitude nulls.

### 3.2 Scatter Modulation and Power Spectra

The over-all backscatter patterns for the unmodulated target have been described. The next aspect is the modulated backscatter at a number of selected angular coordinates. The complete unmodulated backscatter patterns are significant for the selection of appropriate cases. The radar return near nulls will be more sensitive to changes in target structure, but for detection, the strongest return is important. A wide range of elevation and azimuthal conditions are reported here.

In Section 2, discussions of magnitude and phase history calculations were separated from those relating to modulation power spectra determination. In the results, however, the power spectra will be presented together with the associated signal modulation rather than deferred to a later section. The first series of figures shows the variation with azimuth for a given elevation angle. Then for selected azimuthal angles, the variation with elevation angle is depicted. Finally, some results for cross-polarized backscatter at various azimuthal positions are included.

For all cases at both frequencies, there is essentially an unvarying value for the magnitude over a cycle. Thus the figures just show phase variations with the fixed magnitude indicated. The value given is actually expressed as a relative cross section in decibels. The normalizing factor is the corresponding backscatter for an incident signal aligned with the fuselage wires. For the power spectra figures, any component with a value less than -100 dB is indicated by a solid half-circle on the plot at -100 dB.

Figure 7 shows the phase variation for 7-MHz $E_\phi$ polarization at an elevation angle, $\theta = 60°$. Six azimuthal angles are depicted. Since the magnitude is insensitive to the change in configuration, the values just reflect Figure 3b; this applies in general. The 7-MHz fuselage normal backscatter magnitude, $|E_s|_F = 3.04$ V/m. The phase variation changes with azimuth but is always less than one degree. As the angle of incidence nears $\phi = 90°$, we would expect the influence of the fuselage to dominate and indeed the variation from $\phi = 60°$ to $\phi = 120°$ is much less. In all cases, the variation appears to follow the wing deflection.

Figure 8 shows the power spectra for the cases shown in Figure 7. The first and third non-zero frequency components are the strongest in all cases. The dc value in this case is used to represent the return of the carrier frequency of the signal. The strongest values are at $\phi = 30°$ which was the largest phase change case. The spectra have similar variations to those in Figure 7 with the modulation having little effect between $\phi = 60°$ and $\phi = 120°$. For all the cases, the power is relatively weak.

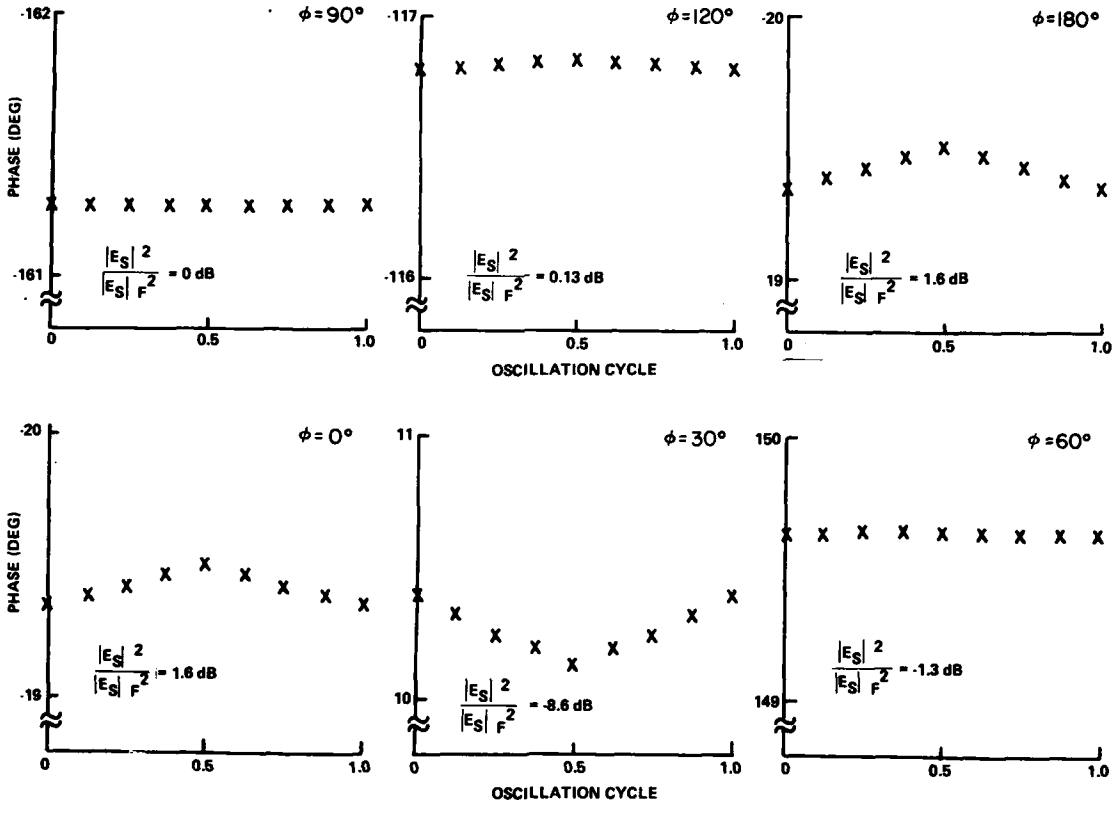


Figure 7. Backscatter Field Over an Oscillation Cycle for 7-MHz, $E_\phi$ Polarization, and Elevation Angle $\theta$ = 60° at Successive Azimuthal Angles

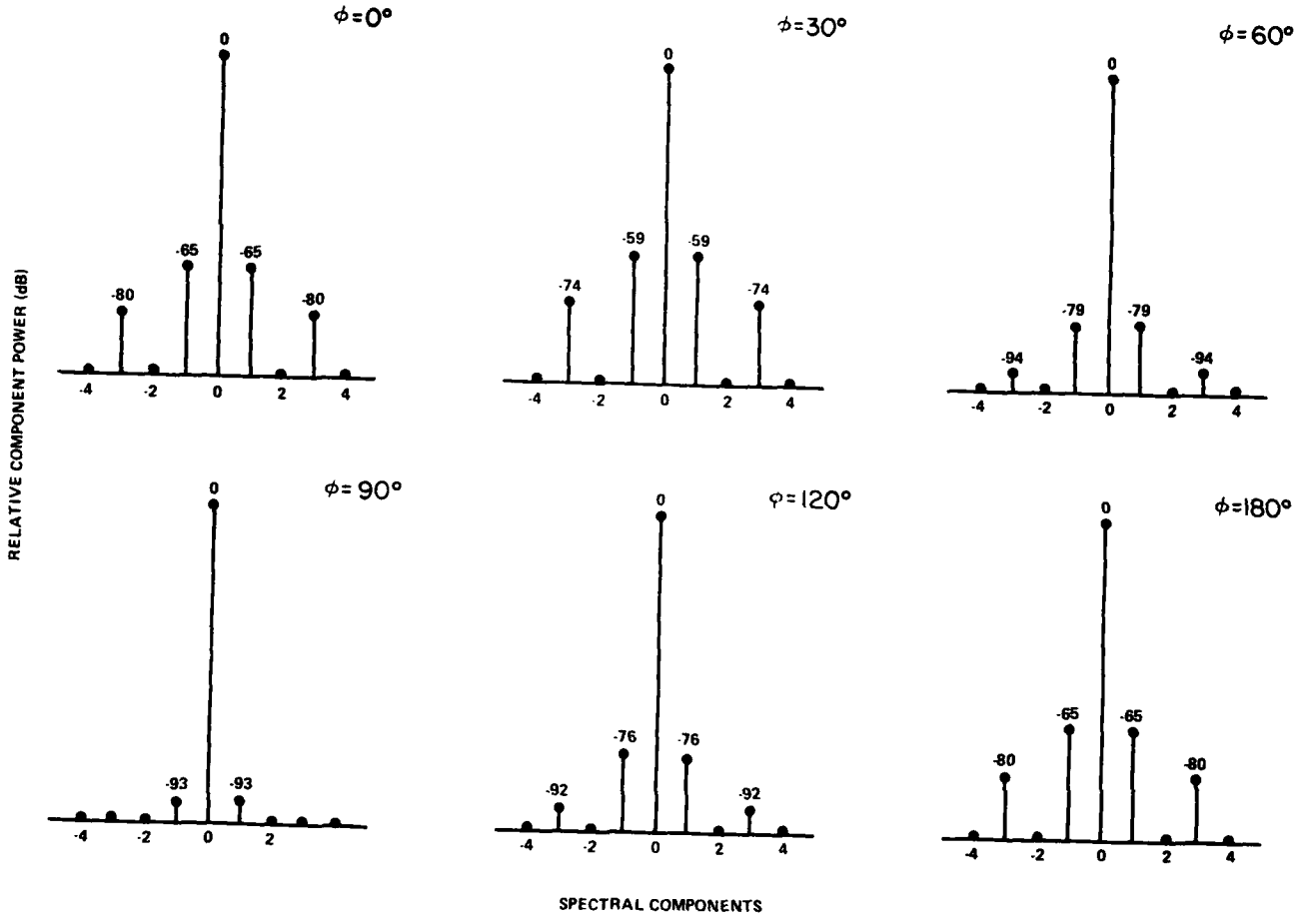


Figure 8. Relative Power Spectra of Signal Frequency Components for 7-MHz, $E_\phi$ Polarized Modulated Signal, and Elevation Angle $\theta$ = 60° at Successive Azimuthal Angles

Figure 9 shows the same phase histories for an $E_\theta$ polarized incident wave. The magnitudes tend to be less than for the $E_\varphi$ polarized cases. The phase changes are on the order of one degree except for the case of $\phi = 60°$. This small variation appears anomalous; it is not present at $\phi = 120°$ which is similar in symmetry with respect to the wing. The $\phi = 60°$ case has the smallest magnitude of these cases but the minimum is near $\phi = 45°$. There, the phase variation is greatest (see Figure 15a). The phase variation follows the wing deflection cycle.

Figure 10 shows the associated power spectra for the cases of Figure 9. The absolute strength of the signal is less than for the $E_\varphi$ polarized case but the non-zero frequency components are more apparent. Again, the dc level is as strong as the unmodulated case and the first and third frequency components are the strongest non-zero frequency terms in the spectra. Relative levels are still quite small.

Figure 11 shows the $E_\phi$ backscatter history for $\theta = 60°$ at 28 MHz. The fuselage normalization magnitude for this frequency, $|E_s|_F = 1.39$ V/m. For all azimuthal angles, the magnitudes are less than the fuselage normal magnitude which is not true for the 7-MHz case. In addition, the absolute magnitudes are less than those at 7 MHz. The phase variation is on the order of one degree over a deflection cycle at $\phi = 90°$ where the fuselage dominates. The effect of wing deflection is still apparent at $\phi = 60°$ and $\phi = 120°$ which is not so for 7 MHz.

Figure 12 shows the associated power spectra. At $\phi = 90°$ the spectra is that of an unmodulated signal to within -100 dB. The same non-zero frequency terms are strong and the dc value is zero dB. There is some contribution from second and fourth components in the spectra but these are far smaller than the main components. The relative strength of the modulation is greater than the 7-MHz case.

Figure 13 presents the $E_\theta$ polarized backscatter histories for 28 MHz and $\theta = 60°$. There is considerable variation in magnitude with azimuth. The $E_\theta$ polarized case for $\phi = 0°$ does exceed the fuselage normal result; this is not true for any $E_\phi$ case. The absolute magnitudes are slightly greater than those for 7 MHz. For $\phi = 60°$ and $\phi = 120°$, the phase variation is on the order of one degree per cycle. The variation for other azimuthal angles is generally less than 0.5°. Where the fuselage dominates the scattering, the phase variation is again minimized. The over-all correlation with wing deflection is apparent.

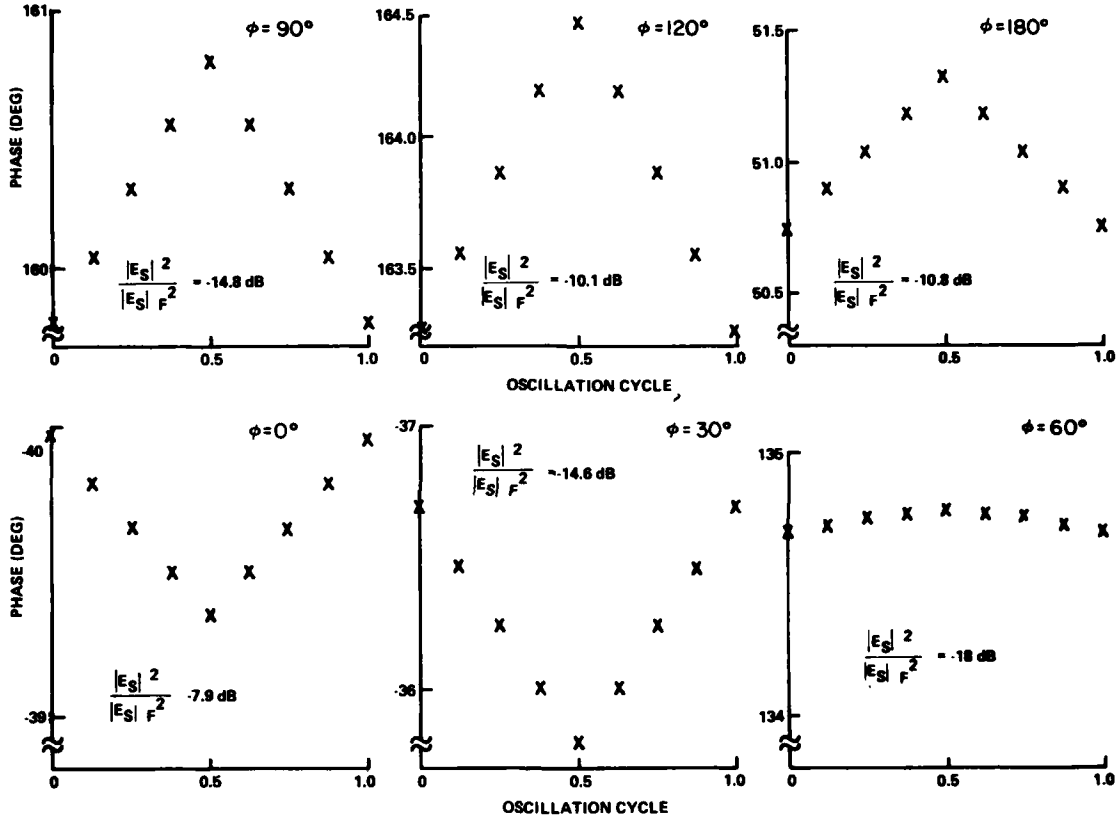


Figure 9. Backscatter Field Over an Oscillation Cycle for 7-MHz $E_\phi$ Polarization, and Elevation Angle $\theta$ = 60° at Successive Azimuthal Angles

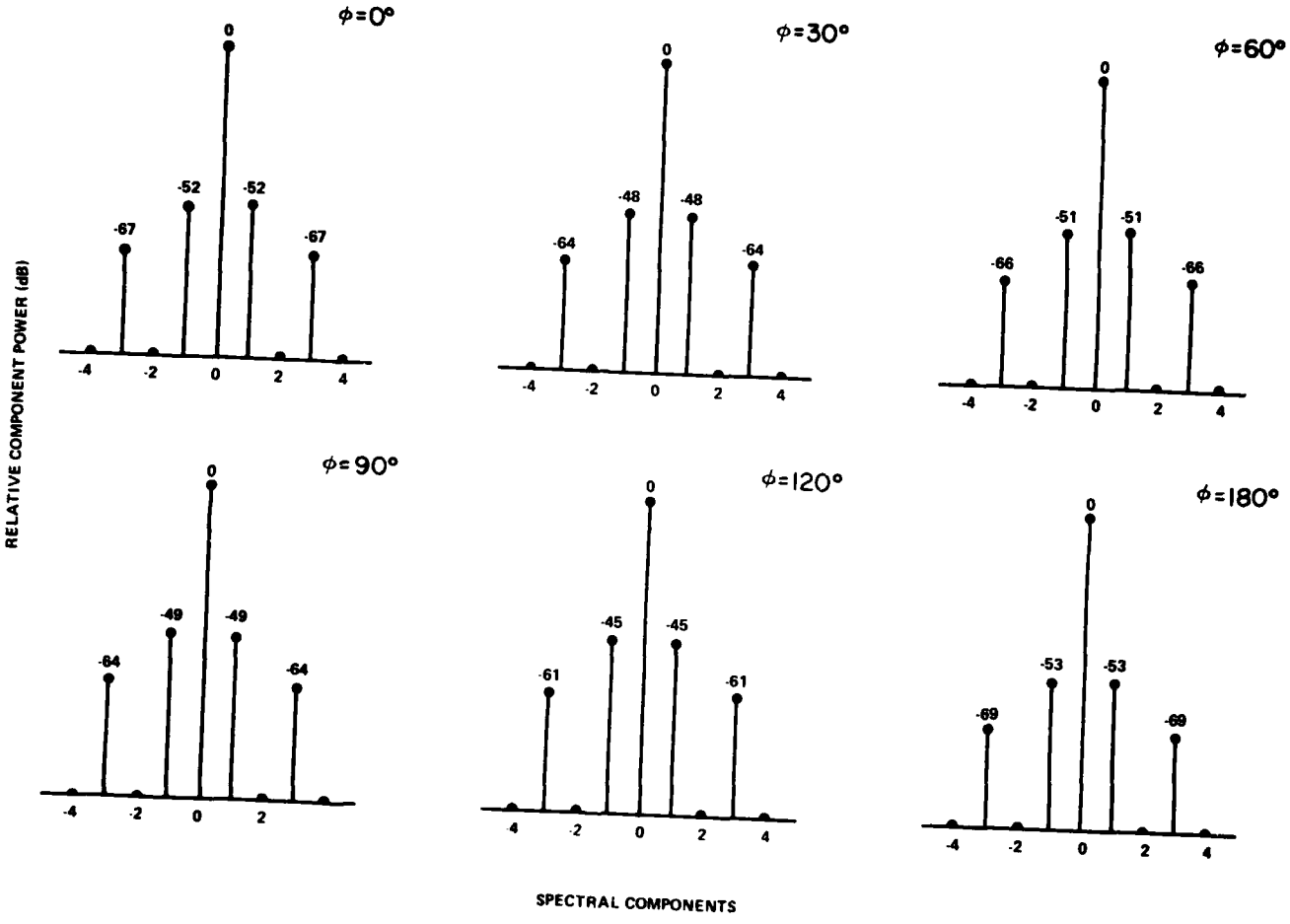


Figure 10. Relative Power Spectra of Signal Frequency Components for 7-MHz, $E_\phi$ Polarized Modulated Signal, and Elevation Angle $\theta = 60°$ at Successive Azimuthal Angles

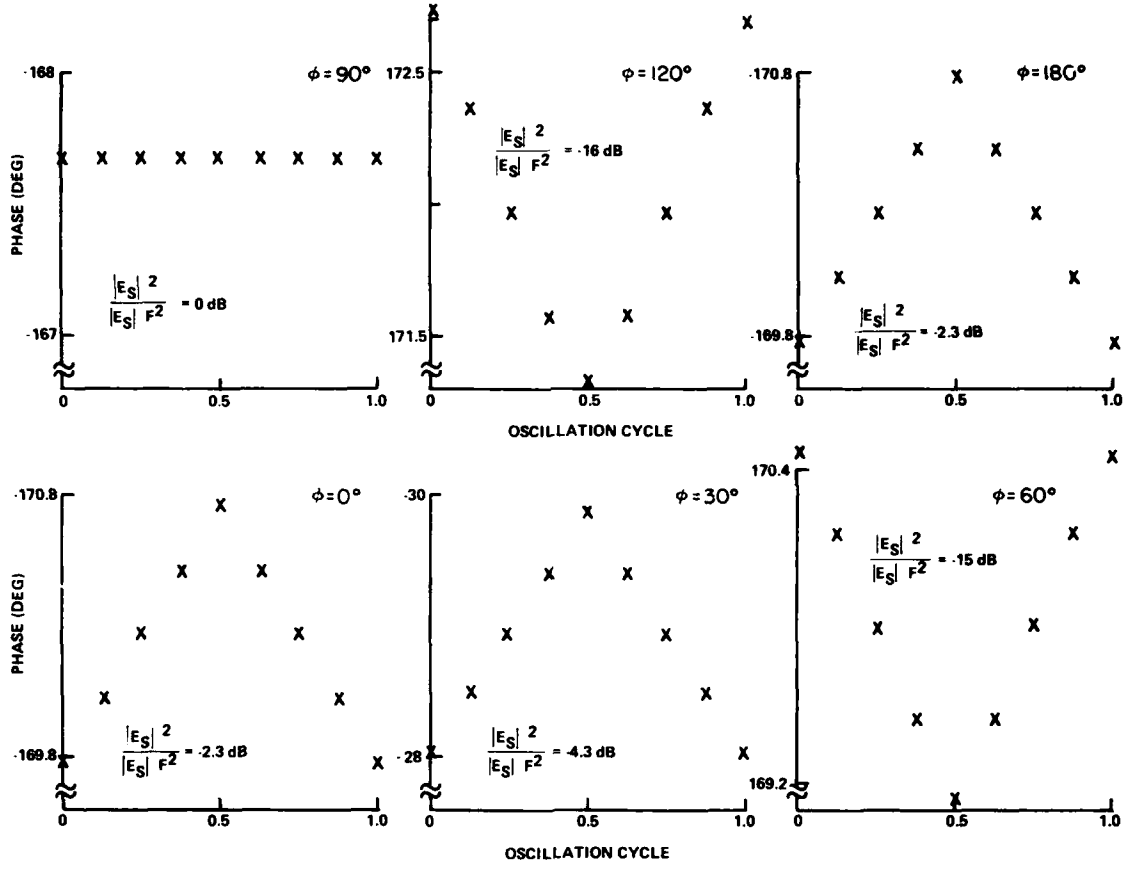


Figure 11. Backscatter Field Over an Oscillation Cycle for 28-MHz, $E_\phi$ Polarization, and Elevation Angle $\theta$ = 60° at Successive Azimuthal Angles

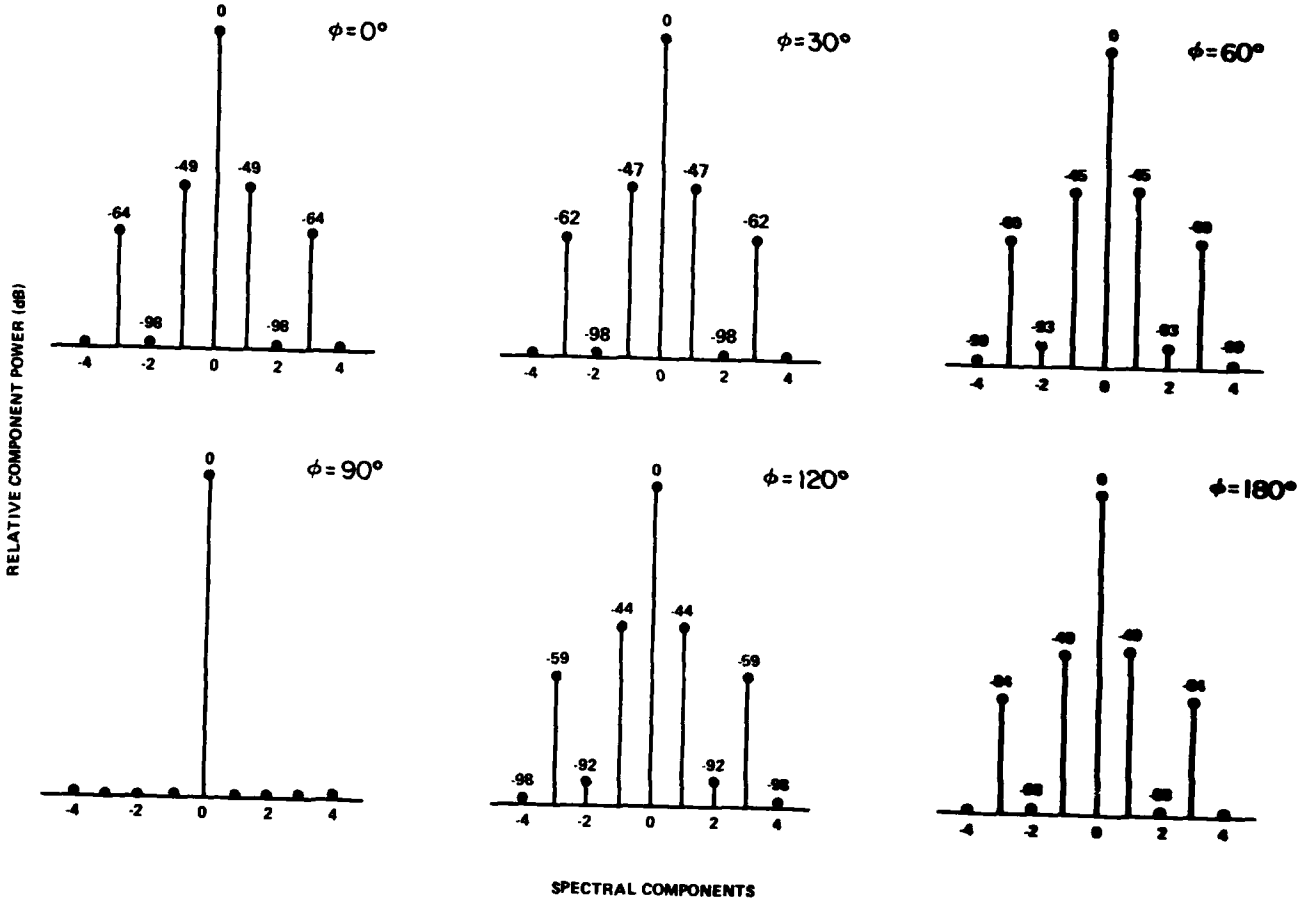


Figure 12. Relative Power Spectra of Signal Frequency Components for 28-MHz, $E_\phi$ Polarized Modulated Signal, and Elevation Angle $\theta$ = 60° at Successive Azimuthal Angles

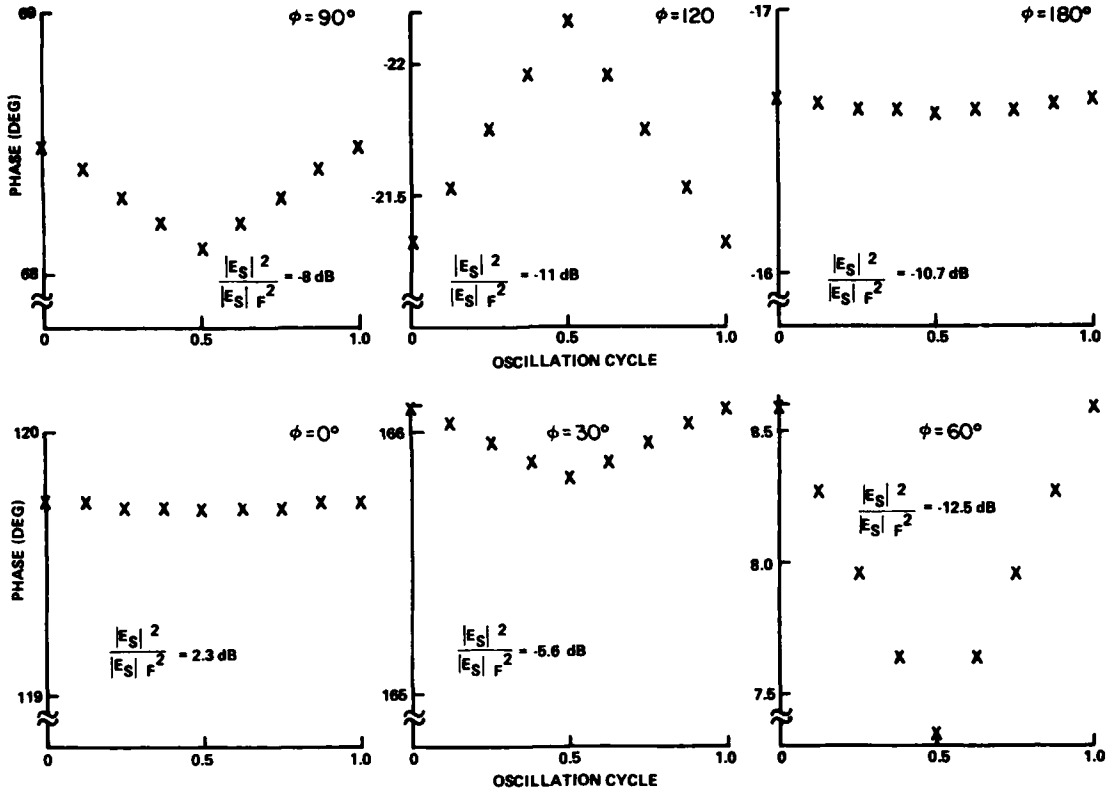


Figure 13. Backscatter Field Over an Oscillation Cycle for 28-MHz, $E_\phi$ Polarization, and Elevation Angle $\theta$ = 60° at Successive Azimuthal Angles

Figure 14 shows the related power spectra. The dc value is essentially that of an unmodulated signal. The sample pattern of first and third component contributions is repeated, as is the suppression of other terms to less than -100 dB. The modulation appears to be as strong as that of the 7-MHz $E_\theta$ case except for $\phi = 0°$ and $\phi = 180°$. The general modulation level appears comparable to the $E_\phi$ polarized case at 28 MHz.

The preceding results represent the azimuthal variation for the modulation at a fixed elevation angle. The next aspect is examination of the variation with elevation angle at selected azimuthal positions.

Figure 15 shows the phase and magnitude for 7-MHz, $E_\theta$ polarization at $\phi = 45°$ and $\phi = 90°$ when the elevation angle $\theta$ varies from 60° to 85°. At $\phi = 45°$, the magnitude for all three elevation angles is low; at $\phi = 90°$, the $\theta = 60°$ case has a stronger return than the other two cases. The size of the phase change for these cases, ranging from one degree to six degrees, corresponds to proximity to a magnitude null.

Figure 16 shows the resultant power spectra. The non-zero frequency components are strong for these cases, showing the sensitivity to the pattern nulls The spectra are similar to all the others except for the higher levels.

Figure 17 shows backscatter variations and related power spectra for 7 MHz and $E_\phi$ polarization, at $\phi = 45°$ and $\phi = 90°$. The magnitudes are greater and correspondingly, the phase variation is much less. The $\phi = 90°$ case was independent of elevation angle, consistent with the scattering being from the fuselage. At $\phi = 45°$, the phase change is inversely proportional to the elevation angle. The modulation is not significant.

Figure 18 shows the 28-MHz $E_\theta$ polarized backscatter variation in the elevation plane for $\phi = 45°$ and $\phi = 90°$. The magnitudes are larger than for the 7-MHz case. The phase changes for $\phi = 45°$ increase with elevation angle from 0.5 degrees to 1.2 degrees peak to peak. At $\phi = 90°$, the variation is less than 0.5 degrees for all elevations. Figure 19 shows the power spectra. Similar, relatively strong patterns can be seen at all angles. Figure 20 shows both results for $E_\phi$ polarization. At $\phi = 45°$, there is little phase variation; the variation decreases with increasing elevation angle. These results are reflected in the power spectra. For $\phi = 90°$, the signal is unmodulated by the wing motion.

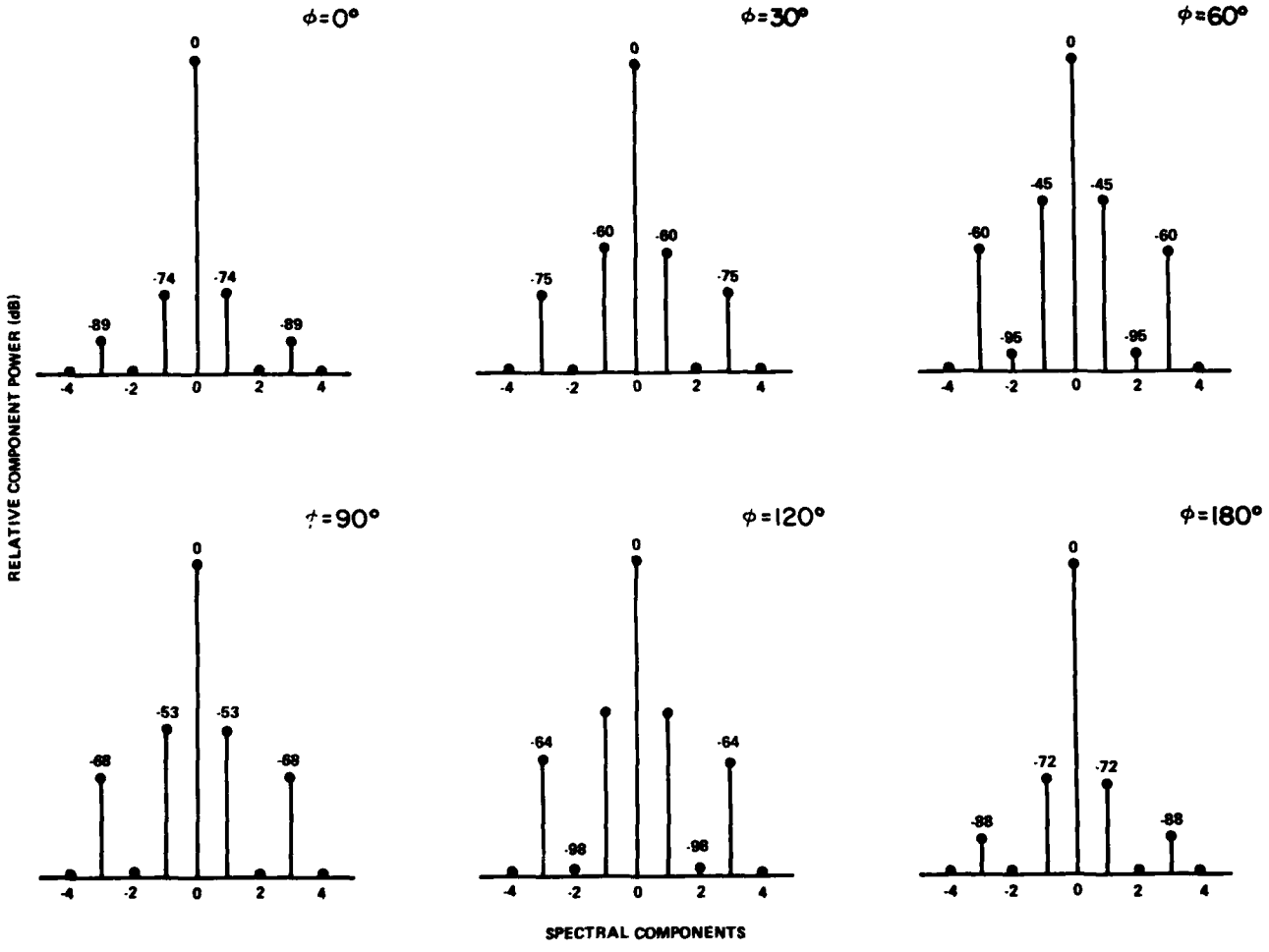


Figure 14. Relative Power Spectra of Signal Frequency Components for 28-MHz, $E_\phi$ Polarized Modulated Signal, and Elevation Angle $\theta$ = 60° at Successive Azimuthal Angle

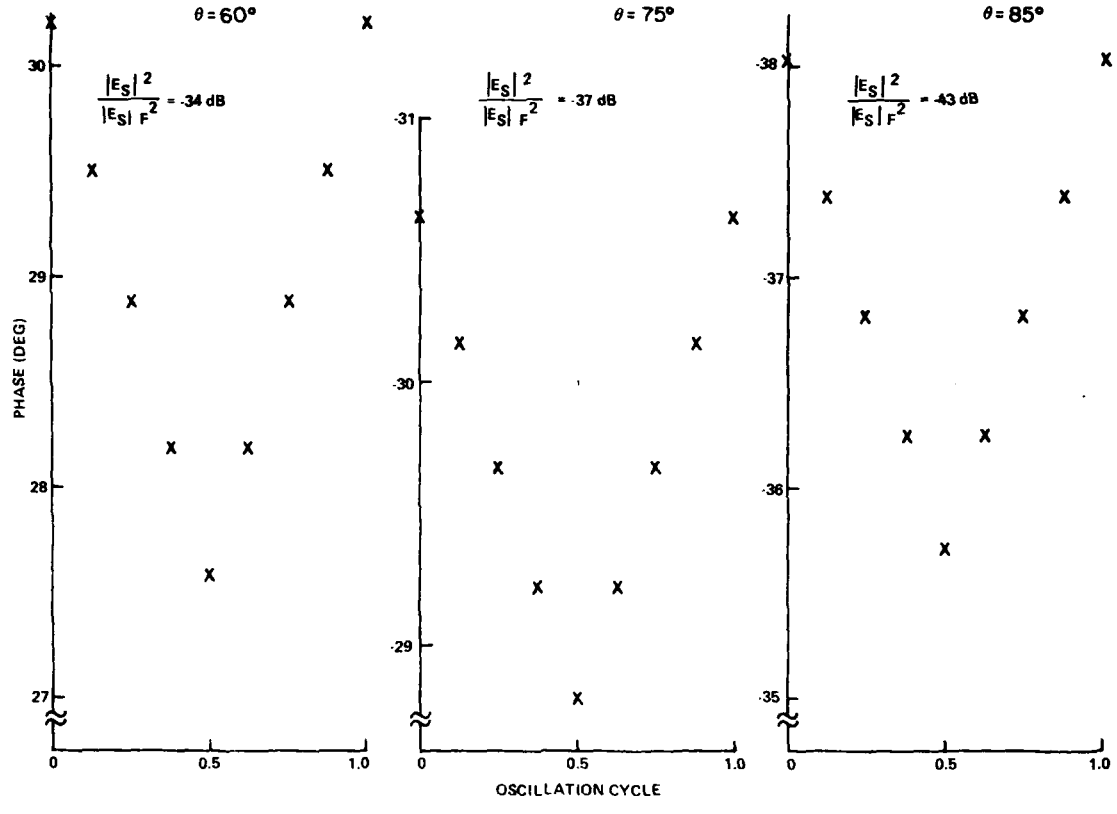


(a)

Figure 15. Backscatter Field Modulation for 7-MHz, $E_\phi$ Polarized Signal and Elevation Angles $\theta$ = 60°, 75°, 85° at: (a) azimuthal angle, $\phi$ = 45° and (b) azimuthal angle, $\phi$ = 90°

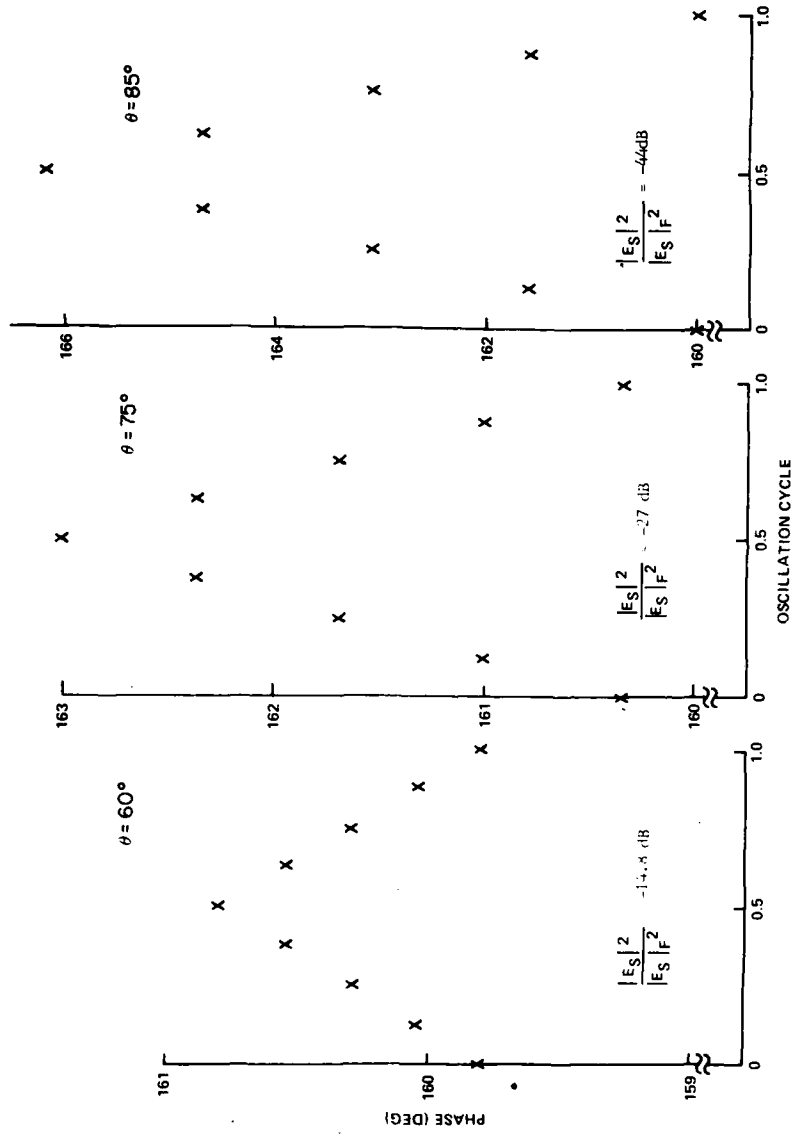


(b)

Figure 15. (Cont)

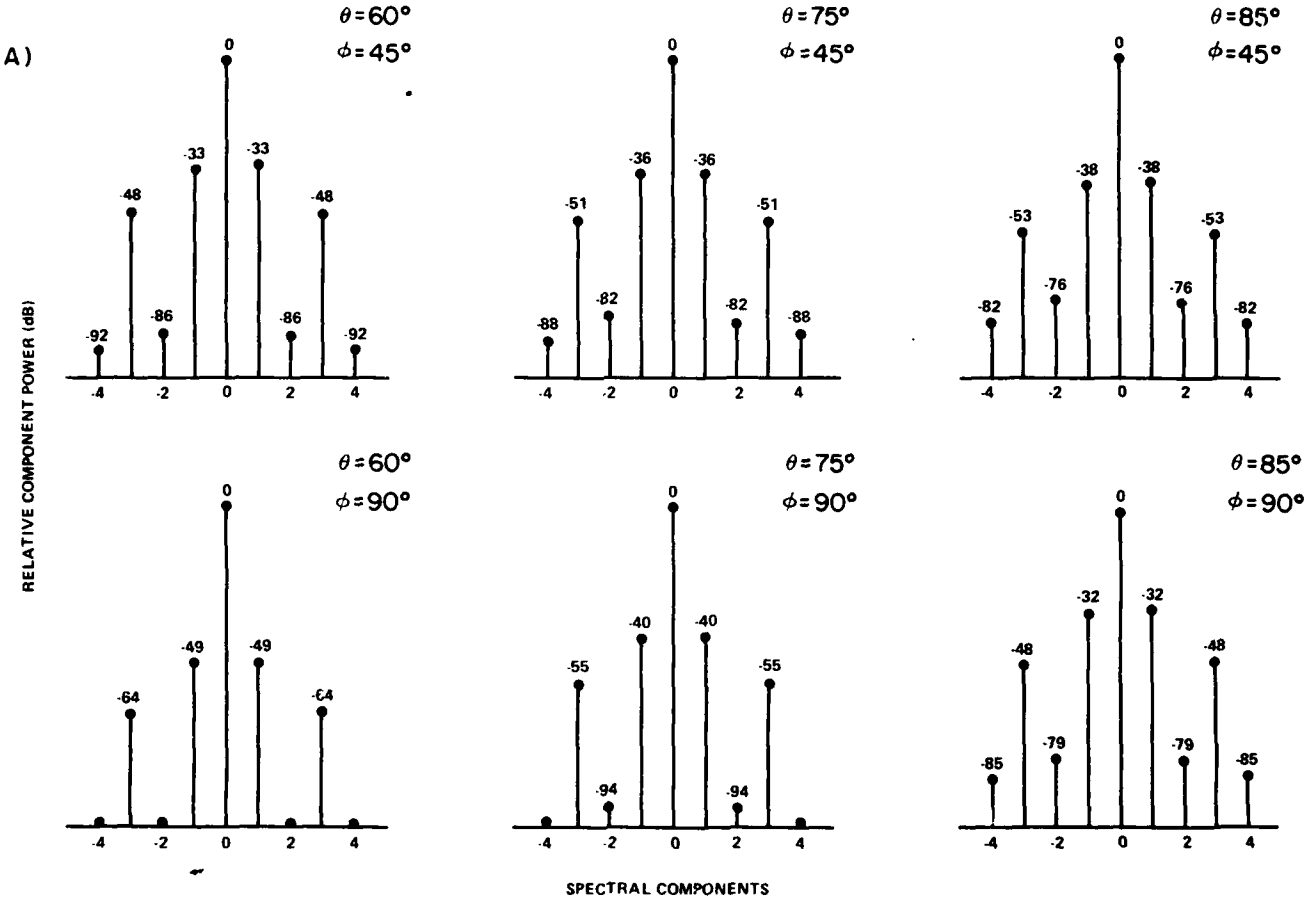


Figure 16. Relative Power Spectra of Signal Frequency Components for 7-MHz, $E_\theta$ Polarization and Elevation Angles $\theta$ = 60°, 75°, 85° at: (a) azimuthal angle, $\phi$ = 45°, and (b) azimuthal angle, $\phi$ = 90°

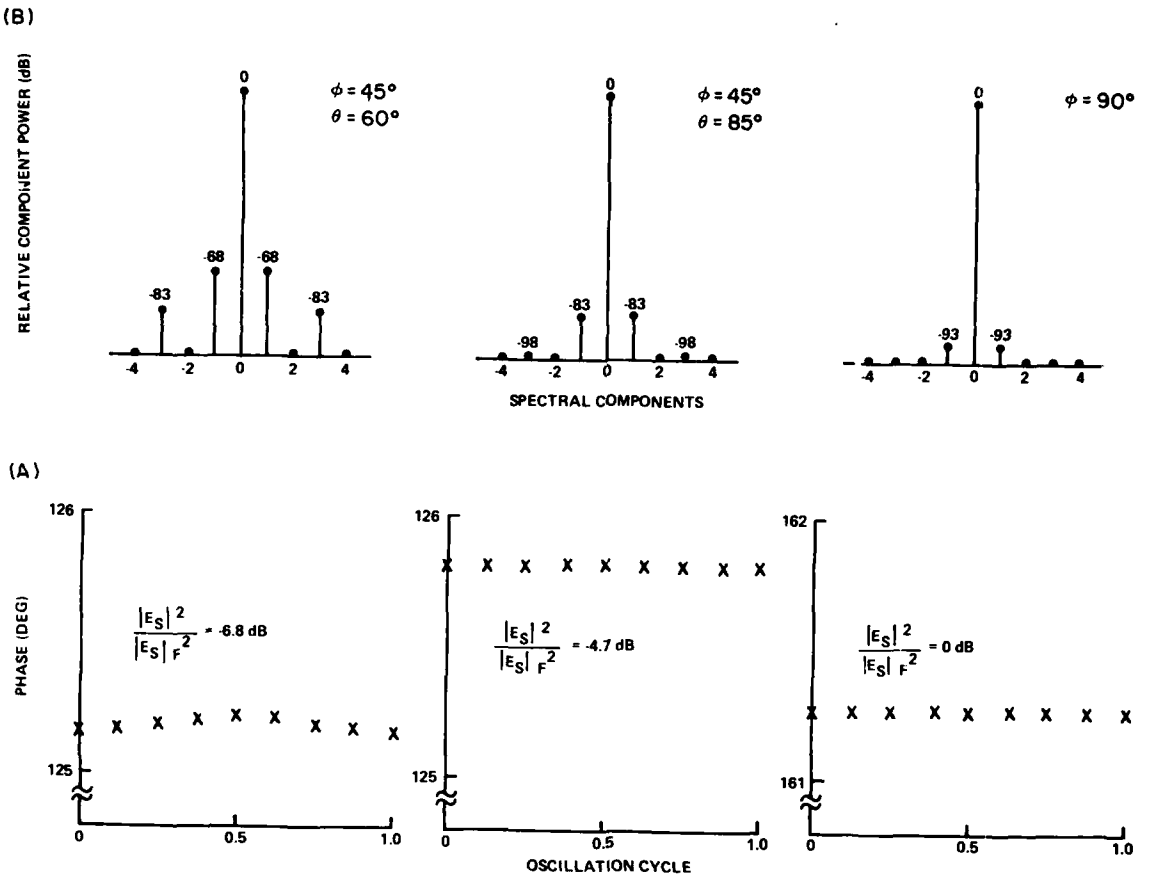


Figure 17. Elevation Angle Effects for 7-MHz, $E_\phi$ Polarized Signal and Azimuthal Angles $\phi$ = 45°, 90° on: (a) signal modulation and (b) power spectra

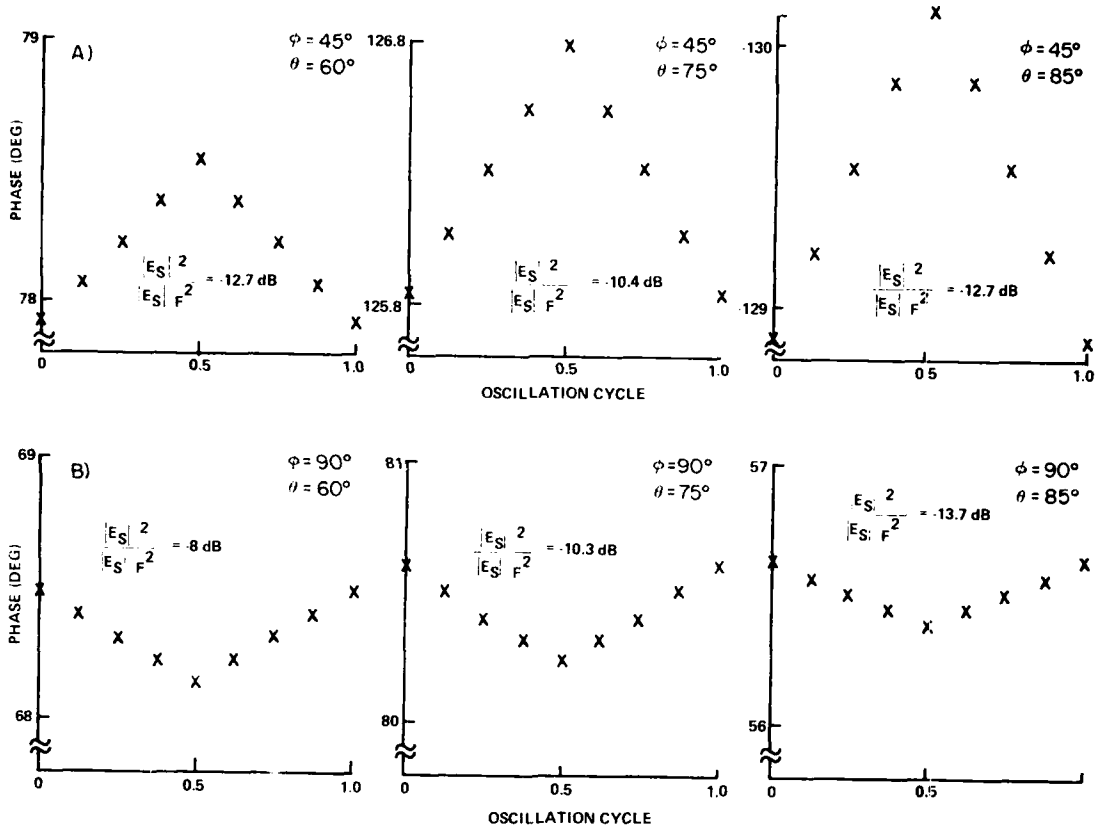


Figure 18. Backscatter Field Modulation for 28-MHz, $E_\theta$ Polarized Signal and Elevation Angles $\theta$ = 60°, 75°, 85° at: (a) azimuthal angle, $\phi$ = 45° and (b) azimuthal angle, $\phi$ = 90°

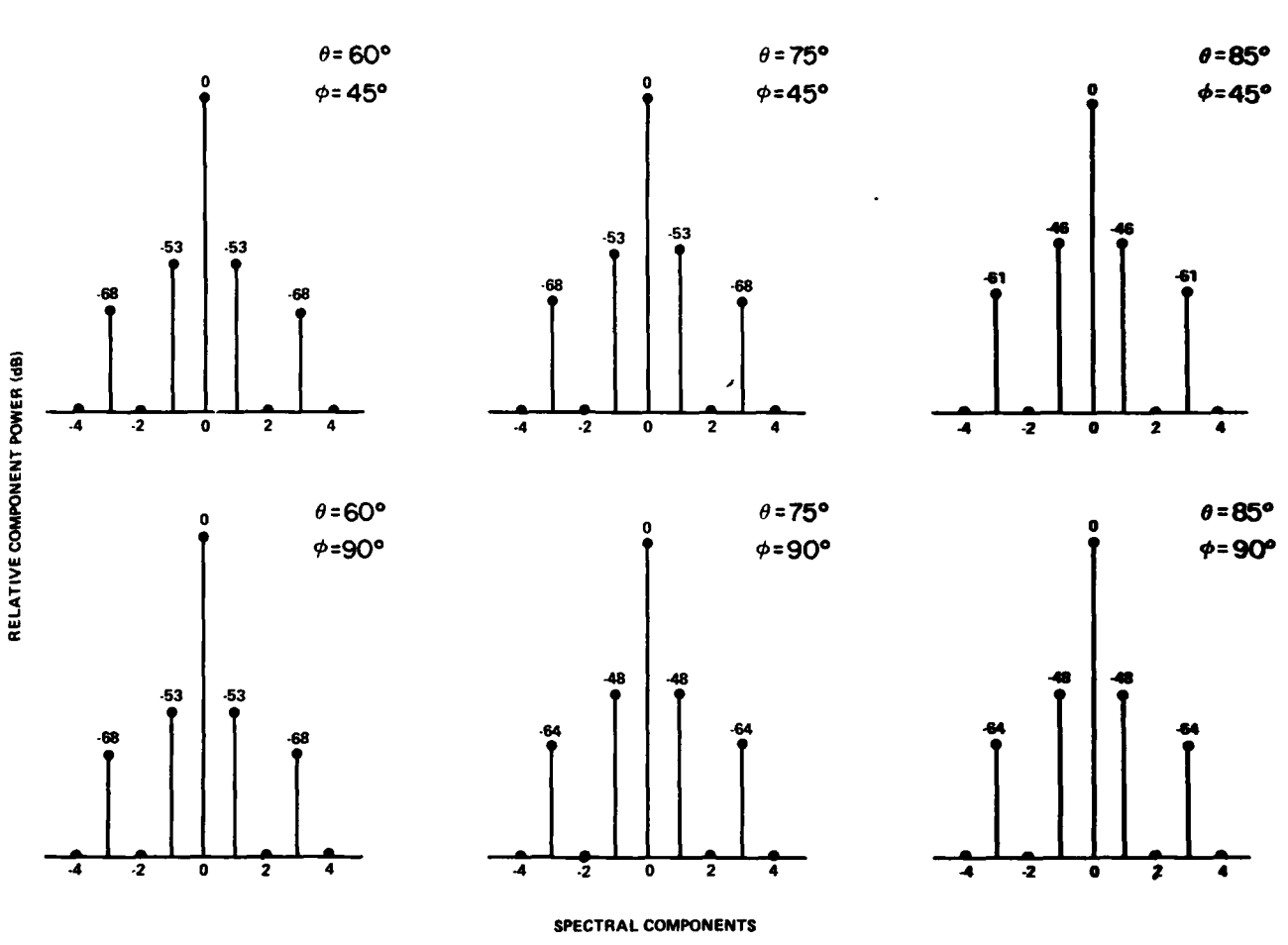


Figure 19. Relative Power Spectra of Signal Frequency Components for 28-MHz, $E_\theta$ Polarization, and Elevation Angles $\theta$ = 60°, 75°, 85° at: (a) azimuthal angle, $\phi$ = 45° and (b) azimuthal angle, $\phi$ = 90°

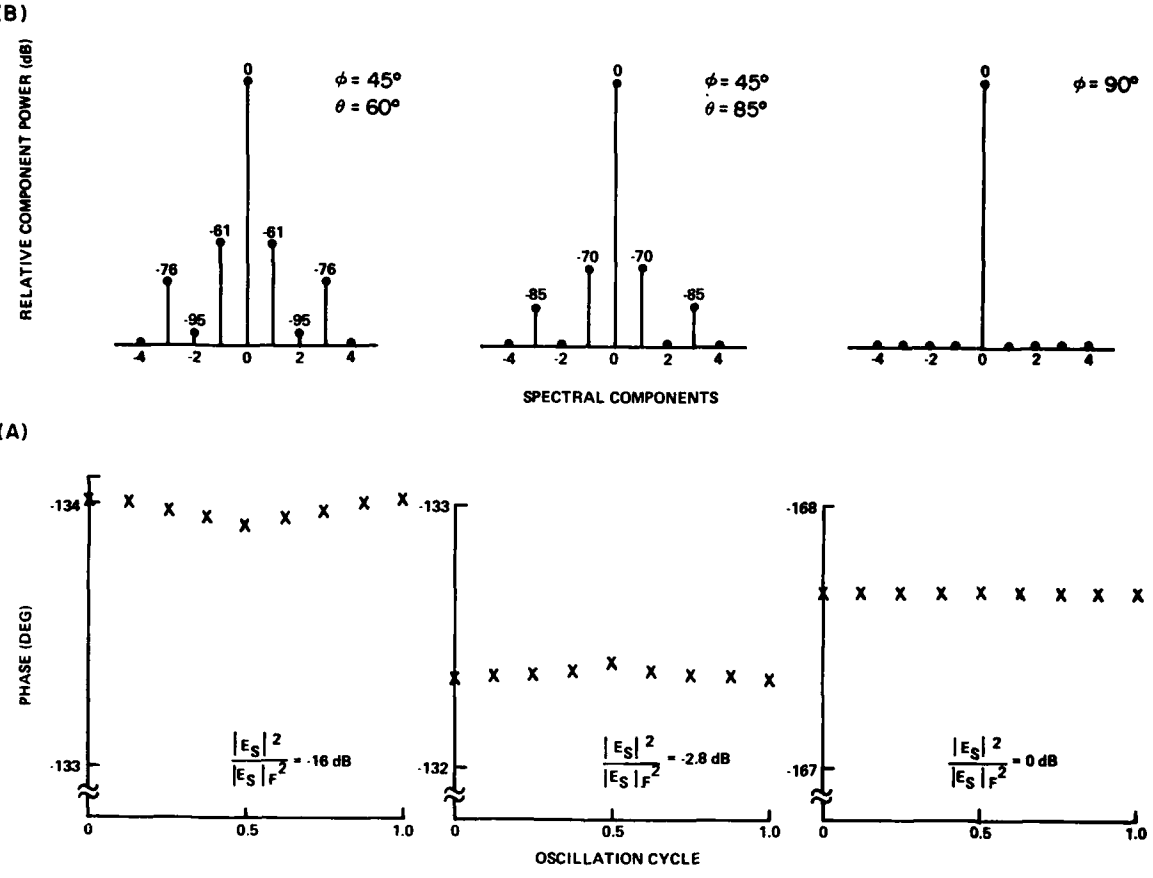


Figure 20. Elevation Angle Effects for 28-MHz, $E_\phi$ Polarized Signal, and Azimuthal Angles $\phi$ = 45°, 90° on: (a) signal modulation and (b) power spectra

The presence of cross-polarized scattering is worth noting. Reciprocity requires the $E_\phi$ polarized incident wave to have the same $E_\theta$ backscatter as the $E_\phi$ backscatter generated by a corresponding $E_\theta$ incident signal.

Figure 21 shows the cross-polarized backscatter and power spectra at 7 MHz for $\theta = 60°$. It should be pointed out that for $\phi = 90°$ and for $\phi = 180°$, there is no cross-polarized backscatter. The magnitude of the cross-polarized scatter has a secondary minimum at $\phi = 90°$ and the phase change is greatest for that case. At $\phi = 90°$ the $E_\phi$ copolarized backscatter ratio has a value of zero dB. The $E_\theta$ copolarized value is -15 dB. The cross-polarized result is also near -15 dB; $\phi = 90°$ corresponds to the strongest nonzero frequency power spectra components.

Figure 22 shows the same results for 28 MHz. Again at $\phi = 0°$ and $\phi = 180°$ there is no cross-polarized backscatter; the secondary minimum is also present at $\phi = 90°$. The greatest phase change per cycle (one degree) occurs at $\phi = 45°$. The power spectra for that angle has slightly stronger modulation components than at $\phi = 90°$. The cross-polarized magnitude ratio is about -10 dB. The corresponding $\phi = 45°$ copolarized backscatter ratio for an $E_\phi$ polarized incident wave is -15 dB and for the $E_\theta$ case it is -13 dB.

At this point we have presented results for various angles, frequencies, and polarizations. One additional aspect of the study remains to be presented: the relationship between some of the discrete results obtained here and those from a simple analytic formulation that contains wing variation as part of the geometry. This is in contrast to the calculations at successive fixed positions that were used to obtain the preceding modulation results. This will be described in the next section.

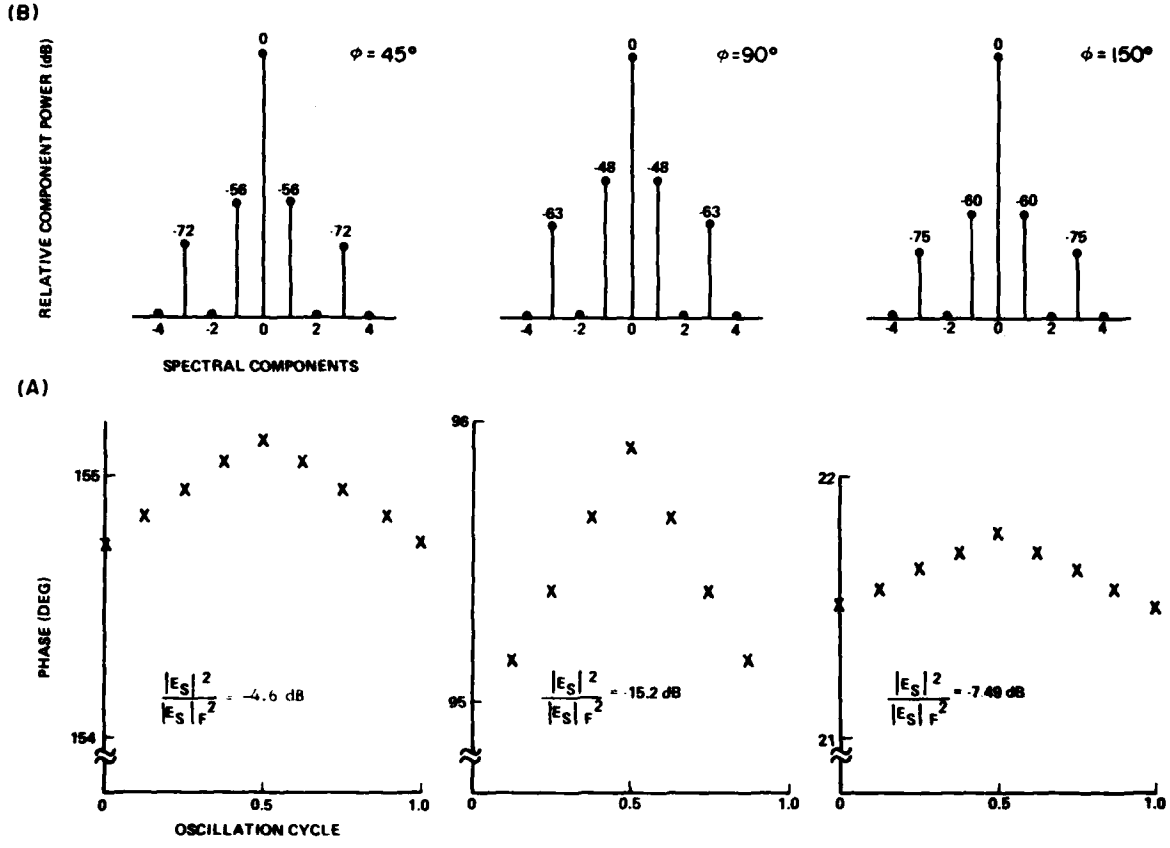


Figure 21. Cross-Polarized Backscatter Field for a 7-MHz Signal at an Elevation Angle $\theta$ = 60° and Azimuthal Angles $\phi$ = 45°, 90°, 150°: (a) signal modulation and (b) power spectra

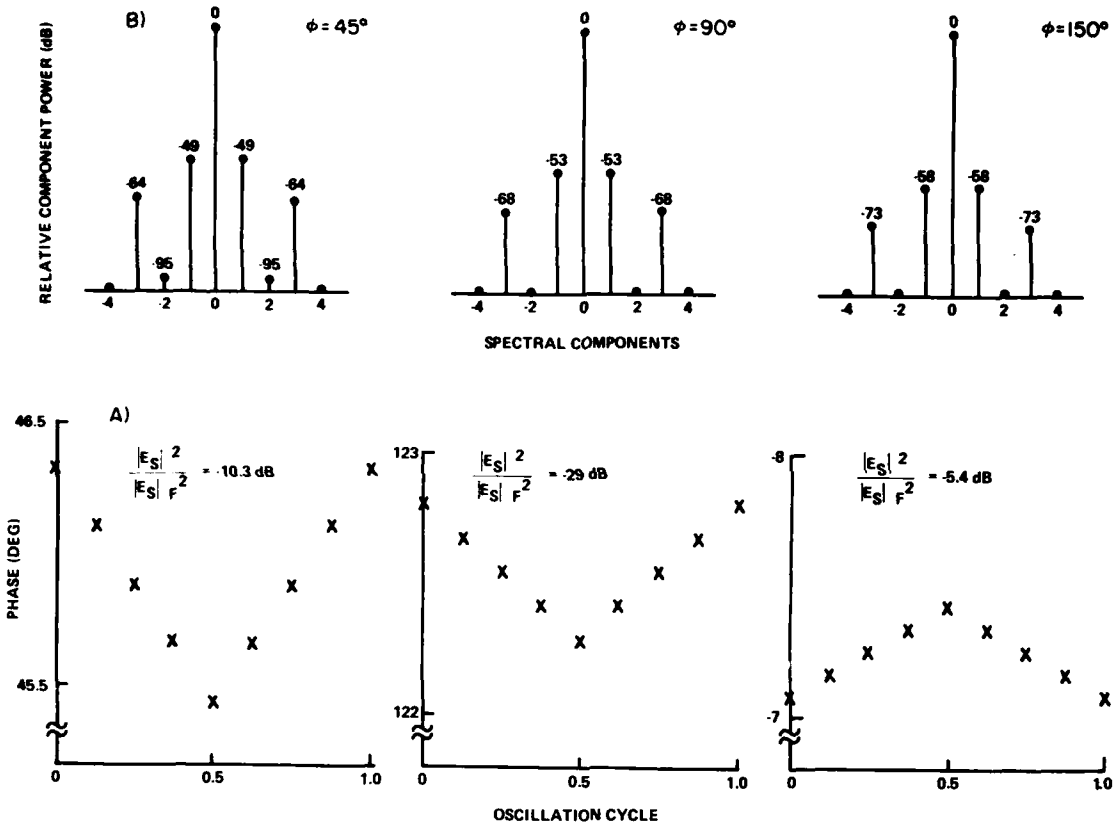


Figure 22. Cross-Polarized Backscatter Field for a 28-MHz Signal at an Elevation Angle $\theta$ = 60° and Azimuthal Angles $\phi$ = 45°, 90°, 150°: (a) signal modulation and (b) power spectra

## 4. DIPOLE MODEL

### 4.1 Theoretical Analysis

For the simple model, we consider the plane wave backscatter from crossed dipoles where the position of the components is not restricted to the x-y plane. Figure 23 shows the equivalent configuration where the angle $\xi$ represents the instantaneous angular variation of the wing wires.

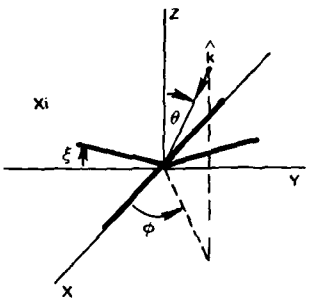


Figure 23. Scattering Model Configuration for the Dipole Theory Showing Scattering Angles ($\theta$, $\phi$) and Cyclic Wing-Dipole Displacement Angle ($\xi$)

The dipoles are considered to be electromagnetically noninteracting and the effect of the time dependent wing deflection is limited to phase changes in the waves reflected from the wings. The complex scatter field $Se^{j\underline{s}}$ then can be described as

$$Se^{j\underline{s}} = F_1 e^{j\underline{f_1}} + W_1 e^{j\underline{w_1(t)}} + W_2 e^{j\underline{w_2(t)}}$$

where the upper case symbols are fuselage and wing-field amplitude factors and the lower case symbols represent the corresponding phase magnitudes for the dipole fields. To calculate the field, we have to assign values to the individual terms of this expression.

First consider the propagation vector $\hat{k}$ and the two spatial vectors $\vec{w}_1$ and $\vec{w}_2$ which describe the location of the phase center of each wing reflector:

$$\hat{k} = \hat{u}_z \cos\theta - \hat{u}_x \sin\theta \cos\phi - \hat{u}_y \sin\theta \sin\phi$$

$$\vec{w}_1 = |w_1| \hat{u}_y \cos\xi + |w_1| \hat{u}_z \sin\xi$$

$$\vec{w}_2 = |w_2| \hat{u}_y \cos\xi + |w_2| \hat{u}_z \sin\xi \ .$$

Since the instantaneous phase of the field reflected from each wing component is given by $2(\hat{k} \cdot \vec{w})$ where $\vec{w} = \vec{w}_1$ and $\vec{w}_2$, we then have:

$$\underset{\sim}{w_1} = 2(2\pi/\lambda)(\vec{w}_1 \cdot \hat{k}) = -(4\pi|w_1|/\lambda)(\sin\xi \cos\theta + \sin\theta \sin\phi \cos\xi);$$

$$\underset{\sim}{w_2} = 2(2\pi/\lambda)(\vec{w}_2 \cdot \hat{k}) = (4\pi|w_2|/\lambda)(\sin\theta \sin\phi \cos\xi - \cos\theta \sin\xi).$$

For relative phase between the wing and fuselage we initially consider $\underset{\sim}{f_1} = 0$. Since we restrict the time dependence to phase effects the amplitude factors are independent of $\xi$ and we use the nondeflected case ($\xi = 0$) amplitude.

To determine the amplitude of each term in the expression for the complex scattered field, the scattering process is considered in several stages. First, the direction of the incident wave is specified. Then, based on the alignment of fuselage and wing dipoles with the polarization of the incident field, the respective incident components are determined. These components generate induced currents on the fuselage and wing wires causing them to reradiate. The resultant scattered components are then projected back into the incident field direction and those amplitudes are used in the scattering terms. To represent this mathematically, we assume equal amplitude factors for both wings:

$$W_1 = W_2 = |W_1|_i |W_1|_s \quad \text{and} \quad F_1 = |F_1|_i |F_1|_s .$$

Now

$$\hat{e}_\theta = \hat{u}_x \cos\theta \cos\phi + \hat{u}_y \cos\theta \sin\phi - \hat{u}_z \sin\theta$$

and

$$\hat{e}_\phi = \hat{u}_y \cos\phi - \hat{u}_x \sin\phi .$$

The $E_\phi$ incident terms are:

$$|F_1|_i = (\hat{e}_\phi \cdot \hat{u}_x) = -\sin\phi; \quad |W_1|_i = \cos\phi$$

and the $E_\theta$ terms are:

$$|F_1|_i = (\hat{e}_\theta \cdot \hat{u}_x) = \cos\theta \cos\phi; \quad |W_1|_i = \cos\theta \sin\phi .$$

For convenience and comparison with the preceding results, we normalize the various amplitude factors with respect to the value for a fuselage normal incident wave, $F_{1N} = 1$. Then the $E_\phi$ polarized backscatter has the form:

$$se^{j\underline{s}} = \sin^2\phi = \left(\frac{\cos^3\phi}{2}\right)\left[\exp\left\{-(j\,4\,\pi\,|W_1|/\lambda)(\cos\theta\ \sin\xi + \sin\theta\ \sin\phi\ \cos\xi)\right\}\right.$$

$$\left. + \exp\left\{-(j\,4\,\pi\,|W_2|/\lambda)(\cos\theta\ \sin\xi - \sin\theta\ \sin\phi\ \cos\xi)\right\}\right]$$

and the $E_\theta$ case is

$$se^{j\underline{s}} = \cos^2\theta\ \cos^2\phi + \left(\frac{\sin^2\phi\ \cos^2\theta}{2}\right)\left[e^{j\,\underline{W}_1(t)} + e^{j\,\underline{W}_2(t)}\right].$$

Here, the phase expressions are not written explicitly.

The corresponding expression for the case of cross-polarized backscatter is

$$s\,e^{j\underline{s}} = -\frac{\cos\theta\ \sin 2\phi}{2} + \frac{\cos\theta\ \sin 2\phi}{4}\left[e^{j\underline{W}_1(t)} + e^{j\underline{W}_2(t)}\right].$$

These are very simple re. ' ons that have a number of possible refinements. For instance, two obvious ones are treating the phase factors on the wings as separate elements (essentially locating the respective phase centers independently) and being more explicit for the fuselage phase term relative to the distinct wing terms. In the actual cases considered here, though, the wing values were kept such that $|W_1| = |W_2|$.

### 4.2 Comparison of Results

First a comparison was made between the results for backscatter patterns at 7 MHz. The wings were fixed at zero deflection ($\xi = 0°$) and the relative amplitude plotted as a function of azimuth for $\theta = 60°$. Figure 24 shows the results for two different phase center values in the Dipole model and the corresponding results for the present computer program. The $E_\phi$ and cross-polarized results are similar, except for the depth of the nulls. There is a large discrepancy though, for the $E_\theta$ polarization results.

Figure 25 shows the cyclic scattering comparisons for various polarizations and angles of incidence. Because of the arbitrary phase definitions, the results are normalized by different values in an attempt to compare the respective amounts of phase change over a deflection cycle. The direct correspondence between phase and deflection can be seen for both models. The amplitude terms in the Dipole model were assumed independent of the modulation.

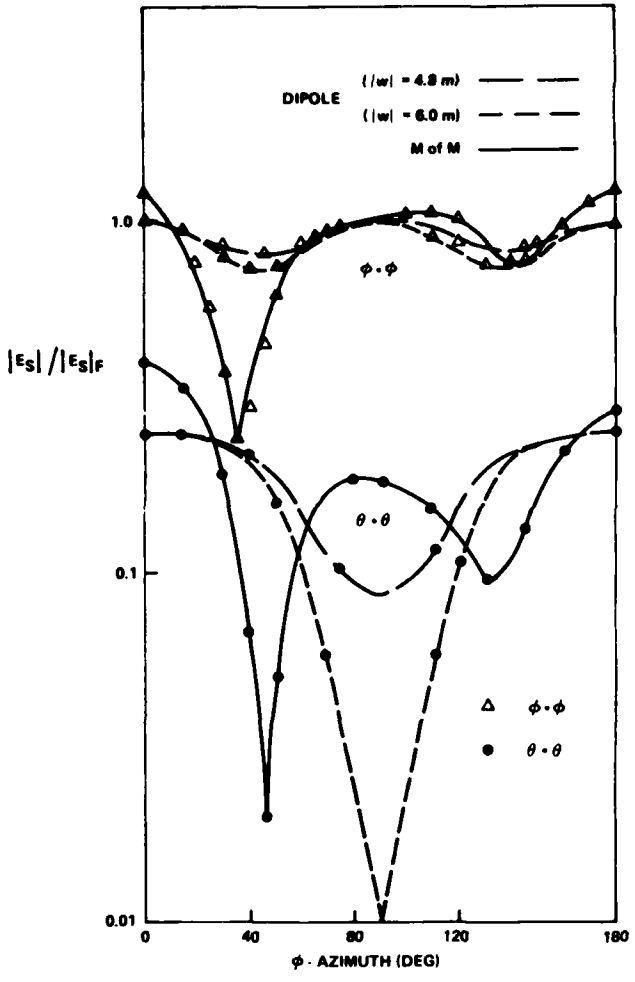


(a)

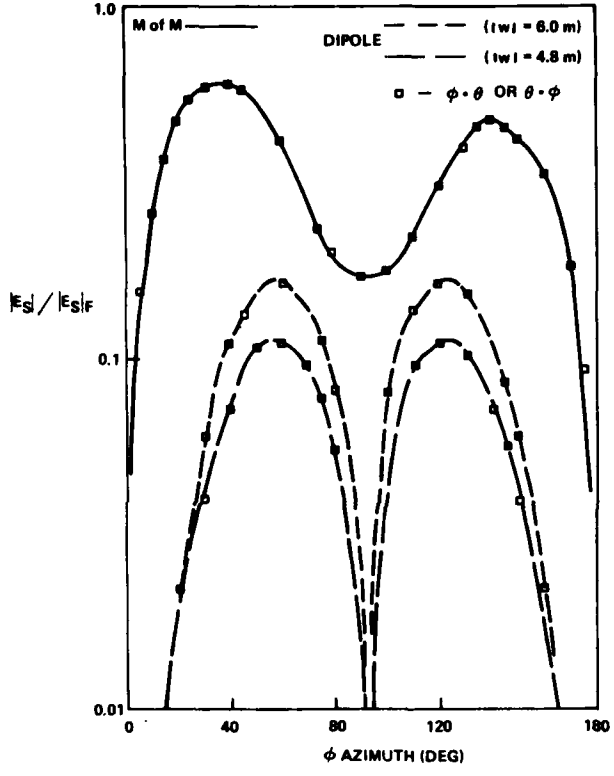


(b)

Figure 24. Azimuthal Plane Backscatter Field Magnitude Pattern Comparison Between the Two Models for 7 MHz, Elevation Angle $\theta$ = 60° and Deflection Angle, $\xi$ = 0°: (a) copolarized and (b) cross-polarized

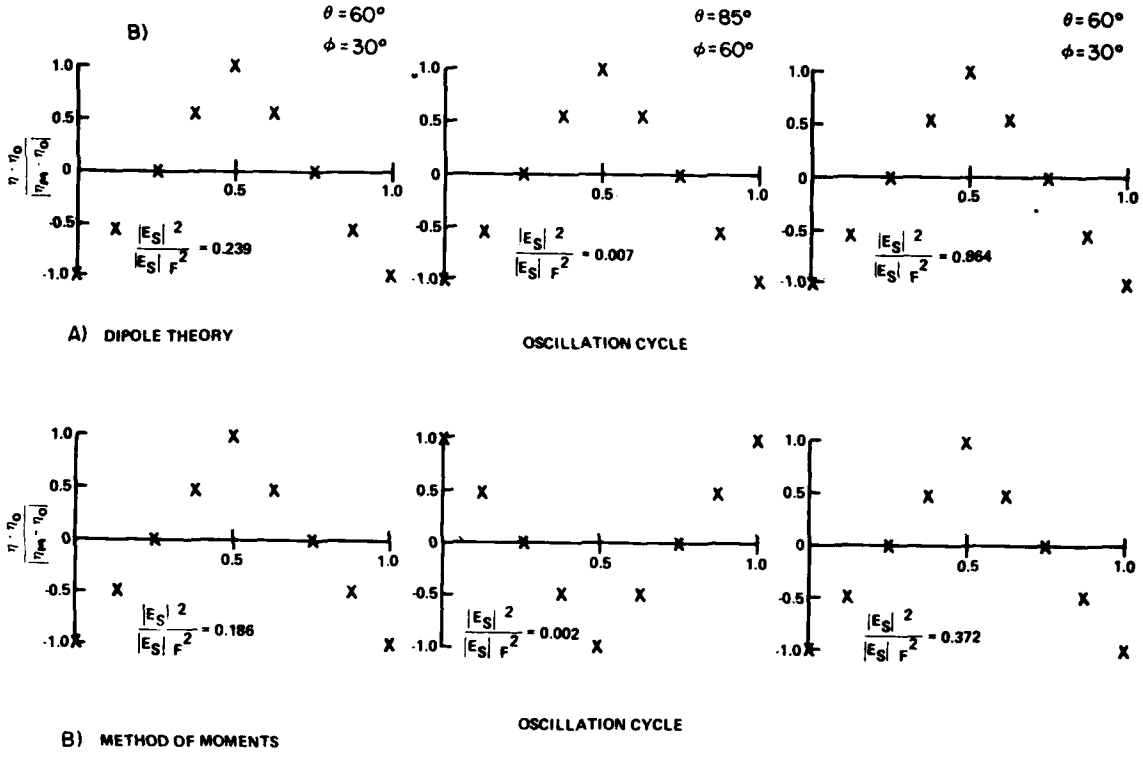


Figure 25. Normalized Phase Variation Over an Oscillation Cycle for a 7-MHz Signal: (a) Dipole theory and (b) method of moments

### 4.3 Discussion

Some justification for a more sophisticated treatment of the relative phase and amplitude values than that provided in the Dipole model can be seen in the wire current distributions produced by the Syracuse University Computer Program. In Figure 26, the currents on the four wires are shown at 7 MHz for $E_\theta$ polarized incident wave at an elevation $\theta = 60°$. The two cases represent azimuth conditions, $\phi = 0°$ and $\phi = 90°$. Positive current conventions are indicated by the arrows. The results are complex. For $\phi = 0°$, there is symmetry for the wing currents, but this is not the case for $\phi = 90°$ as would be expected, since there is a tail contribution. Thus, it is not surprising that the Dipole model was considerably at variance with results for these $E_\theta$ polarized scattering cases. Separate adjustment of phase center locations may lead to better agreement, but this has not been pursued.

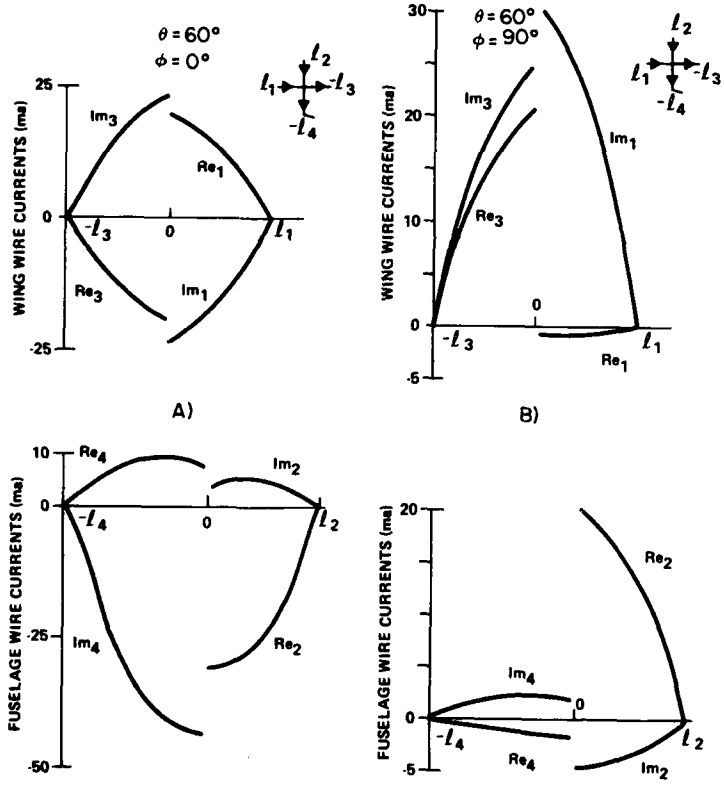


Figure 26. Complex Currents Induced on the Wires in Method-of-Moment Solution for a 7-MHz, $E_\theta$ Polarized Signal, and Elevation Angle $\theta = 60°$. Arrows indicate direction convention for positive current at: (a) azimuthal angle $\phi = 0$ and (b) azimuthal angle $\phi = 90°$

In an attempt to examine the form of the cyclic variation in phase, an analysis of the phase expression of the Dipole model was carried out assuming deflection angles, $\xi \leq 1°$, appropriate for the aircraft data of this study. The result shows that the normalized phase dependency can indeed be written as

$$\eta / |\eta_0| = -\xi / |\xi_0| .$$

This is valid for both cross and copolarized conditions.

## 5. CONCLUSIONS

### 5.1 Related Results

To place the present results in perspective, a brief summary of some of the related results from the University of Michigan study[3] may prove useful. Assessment of the state of the art of identification based on airframe deflections should include consideration of those results.

The University of Michigan found that airspeed has a moderate effect on frequencies and deflection modes for the three types of fighter aircraft studied. Fuel and armament loads (particularly on the wings) have a strong effect. The swing-wing fighter bomber class (to which the F-111 would belong) has a fundamental mode (predominantly fuselage bending) that is insensitive to load variations. The more conventional classes appear to have complicated elastic modes that are sensitive to operating conditions and probably not useful for recognition.

When the elastic modes are translated into airframe deflections, the results are quite small. For the one aircraft with a persistent fundamental model, deflections were further transformed into relative scattering center motion by the University of Michigan. A dynamic radar cross section (RCS) history for the aircraft was obtained in the vertical plane of symmetry at $\lambda$ = 3 cm and $\lambda$ = 30 cm.

At other than nose-on aspect angle, there are signs of RCS modulation related to the fundamental and third harmonic of the dominant vibrational mode of the aircraft. The results at $\lambda$ = 30 cm are not likely to be observable but at $\lambda$ = 3 cm, the modulation contributions might be detectable.

The basic conclusion at the completion of this study is that, although in the one case some airframe related radar modulations might be detectable at $\lambda$ = 3 cm, it is unclear how the over-all results for the characteristic frequency patterns and deflections for a range of aircraft could be used in a realistic identification scheme.

### 5.2 Present Results

The present study is concerned with the radar modulation from the aspects of detection and dependence on incident angle. In contrast to the Michigan study, phase as well as RCS was considered. The significance of the following results has to be discussed in this context:

1. Azimuthal variations in the magnitude of the unmodulated signal show considerable differences, depending on incident polarization and frequency. This is particularly true for the angle of interest, $60° \leq \phi \leq 120°$. For 28 MHz, $E\phi$ polarization, the variation is -15 to 0 to -17 dB, whereas for 7 MHz the relative magnitudes are greater than -1 dB for those angles. For $E_\theta$ polarization, at both frequencies, the relative magnitudes are below -8 dB over that range. The dependence of results on frequency can also be seen in the phase variations. The 7 MHz, $\theta = 60°$, $E\phi$ case has a larger phase variation than does the $E\theta$ polarized result. At 28 MHz, the reverse is true.

2. Large phase variations over a cycle tend to correlate with nulls in the pattern, except for angles where either the wings or the fuselage may dominate the scatter.

3. The phase change per cycle is small; that is, on the order of one degree or less, peak to peak.

4. The phase changes follow the deflection position of the wings for all cases and thus are related to the vibrational frequency.

5. The power spectra are similar for all cases, with strong dc value and contributions generally at the first and third harmonics of the deflection frequency.

6. The power spectra, in terms of range, for all the cases indicate that, compared to the range for detecting the aircraft at a given set of conditions, the aircraft would have to be at about one-tenth that distance or closer in order to detect the modulation.

No consistent span of relatively reasonable modulation levels exists for the angles where engine identification is unreliable, so there is no clear advantage to the use of airframe effects to complement more conventional techniques.

8. Variations in phase and power in the elevation plane tend to be strongest where the magnitude of the signal is small.

9. The patterns for frequencies and polarizations show relatively strong symmetry about the yaw plane. Thus, there is no reason to expect any different results for the case where the incident wave was at an elevation angle below the target.

10. Cross-polarized backscatter does not appear to have any benefit over the copolarized results.

11. The Dipole model does seem to offer an opportunity to substantiate and extend some of the results. However, the discrepancies and the need to make use of external information about current distributions make its use both cumbersome and uncertain.

### 5.3 Assessments

In the context of detection and identification, the extreme variability and stringent range limitations found in this study would make further pursuit with more sophisticated models and higher frequency values seem unreasonable. There are no apparent advantages over engine identification techniques.

On the basis of these results and those from the University of Michigan, that there are no persistent frequency patterns for most aircraft, it is recommended that this research not be pursued further. There would seem to be no point in investigating the recognition problem, since unique, consistent information would not be available for analysis.

## References


1. Hynes, R., and Gardner, R. E. (1967) Doppler spectra of S-band and X-band signals, Supplement to IEEE Trans. Aerospace and Electrical Systems AES-3:356-365.
2. Newburgh, R. G. (1978) Basic Investigations of the Radam Effect, RADC-TR-78-151, AD A058099.
3. Anderson, W. G., Sengupta, D., and Correa, S. (1979) Inflight Aircraft Vibration Modes and their Effect on Aircraft Radar Cross-Section, RADC-TR-79-72
4. Kuo, D. C., and Strait, B. J. (1972) Improved Programs for Analysis of Radiation and Scattering By Configurations of Arbitrarily Bent Thin Wires, AFCRL-TR-72-0051, AD 739203.
5. Lin, Y. T., and Richmond, J. H. (1975) EM modeling of aircraft at low frequencies, IEEE Trans. Antennas and Propagation AP-23:53-56.
6. Chao, H. H., and Strait, B. J. (1970) Computer Programs for Radiation and Scattering by Arbitrary Configurations of Bent Wires, AFCRL-TR-70-0374, AD 713156.
7. Harrington, R. F. (1967) Matrix methods for field problems, Proc. IEEE 55:136-149.
8. Chao, H. H., Strait, B. J., and Taylor, C. D. (1971) Radiation and scattering by configuration of bent wires with junctions, IEEE Trans. Antennas and Propagation AP-19:701-702
9. Uhrich, M. L. (1969) Fast Fourier transforms without sorting, IEEE Trans. Audio and Electroacoustics AU-17:170-172.

| | |
|---|---|
| $a$ | Wire radius (m) |
| $E_\phi$, $\hat{e}_\phi$ | Phi Polarized Electric Field Component and its unit vector |
| $E_\theta$, $\hat{e}_\theta$ | Theta Polarized Electric Field Component and its unit vector |
| $F_{(\omega)}$ | Fourier transform in frequency domain |
| $F_1$ | Fuselage dipole field amplitude factor |
| $f$ | Frequency |
| $f(t)$ | Time function |
| $f_1$ | Phase magnitude for fuselage dipole field |
| $\tilde{K}$ | Unit propagation vector |
| $L$ | Wire length |
| $\ell_s$ | Wire segment length |
| $N$ | Number of signal sample points per cycle |
| $P_{(\omega)}$ | Power spectra |
| $R$ | Range |
| $T$ | Sample period |
| $t$ | Time |
| $\hat{u}$ | Unit vector along Cartesian coordinate axes |
| $W_1$, $W_2$ | Electric field dipole amplitude factor for each wing |
| $w_1$, $w_2$ | Phase magnitudes for the wing dipole fields |
| $\lvert\tilde{W}_1\rvert$, $\lvert W_2\rvert$ | Distance along wing to scattering center |
| $x$ | Fuselage Cartesian coordinate |
| $y$ | Wing Cartesian coordinate |
| $z$ | Tail Cartesian coordinate |
| $\eta_0$ | Phase angle when the wing deflection angle, $\xi = 0°$ |
| $\eta_{max}$ | Maximum phase value |
| $\theta$ | Elevation angle; polarization direction |
| $\lambda$ | Wavelength |
| $\xi$ | Deflection angle for wing |
| $\sigma_{mod}$ | Radar cross section associated with modulation |
| $\sigma_0$ | Unmodulated radar cross section for target |
| $\phi$ | Azimuthal angle; polarization direction |
| $\omega$ | Radian frequency ($2\pi f$) |

# *MISSION*
# *of*
# *Rome Air Development Center*

*RADC plans and executes research, development, test and selected acquisition programs in support of Command, Control Communications and Intelligence ($C^3I$) activities. Technical and engineering support within areas of technical competence is provided to ESD Program Offices (POs) and other ESD elements. The principal technical mission areas are communications, electromagnetic guidance and control, surveillance of ground and aerospace objects, intelligence data collection and handling, information system technology, ionospheric propagation, solid state sciences, microwave physics and electronic reliability, maintainability and compatibility.*

**Printed by**
**United States Air Force**
**Hanscom AFB, Mass. 01731**